CATÓLICA
ESCOLA SUPERIOR DE BIOTECNOLOGIA
PORTO

MEMBRANAS DE QUITOSANO-ÁCIDO HIALURÓNICO RETICULADAS COM UM NOVO AGENTE RETICULANTE DERIVADO DO ÁCIDO FÍTICO

por
Filipe Alexandre Monteiro Barbosa

Julho 2017

CATÓLICA
ESCOLA SUPERIOR DE BIOTECNOLOGIA
PORTO

CHITOSAN-HYALURONIC ACID MEMBRANES CROSSLINKED WITH A NOVEL CROSSLINKING AGENT DERIVED FROM PHYTIC ACID

by
Filipe Alexandre Monteiro Barbosa

July 2017

CATÓLICA
ESCOLA SUPERIOR DE BIOTECNOLOGIA
PORTO

MEMBRANAS DE QUITOSANO-ÁCIDO HIALURÔNICO RETICULADAS COM UM NOVO AGENTE RETICULANTE DERIVADO DO ÁCIDO FÍTICO

Tese apresentada à Escola Superior de Biotecnologia da Universidade Católica Portuguesa para obtenção do grau de Mestre em Engenharia Biomédica

_____

por
Filipe Alexandre Monteiro Barbosa

Local: Escola Superior de Biotecnologia da Universidade Católica Portuguesa

Orientação: PhD Julio San Román
PhD Blanca Vasquez Lasa

Julho 2017

CATÓLICA
ESCOLA SUPERIOR DE BIOTECNOLOGIA
PORTO

CHITOSAN-HYALURONIC ACID MEMBRANES CROSSLINKED WITH A NOVEL CROSSLINKING AGENT DERIVED FROM PHYTIC ACID

Thesis presented to Escola Superior de Biotecnologia of the Universidade Católica Portuguesa to fulfill the requirements of Master of Science degree in Biomedical Engineering

_____

by

Filipe Alexandre Monteiro Barbosa

Place: Escola Superior de Biotecnologia da Universidade Católica Portuguesa

Supervision: PhD Julio San Román
PhD Blanca Vasquez Lasa

July 2017

Resumo

A cartilagem adulta é muito susceptível a lesões à medida que o tempo progride devido à sua espessura, natureza avascular e aumento da apoptose. Além da osteoartrite estar ligada ao envelhecimento populacional, é importante notar que este tipo de lesão articular ocorre freqüentemente na juventude. Independentemente da causa, a degeneração da cartilagem articular pode resultar em problemas irreversíveis. As opcções de tratamento actuais são agressivas para o paciente ou ainda estão em desenvolvimento.

Com isto em mente, é de importância extrema continuar a pesquisar e desenvolver soluções mais viáveis para ajudar a regenerar este tipo de tecido restaurando a sua funcionalidade.

O presente trabalho descreve membranas novas, estáveis e biodegradáveis de proteínas e/ou polissacarídeos, particularmente de quitosano e quitosano/ácido hialurónico, úteis como *scaffolds* para engenharia de tecido ósseo.

Estas membranas foram fabricadas através de misturas de polissacarídeos e proteínas de interesse utilizando novos agentes de reticulação consistindo de derivados de ácido fítico (PA) obtidos a partir de uma reação de condensação entre o ácido fítico e um composto hidroxílico.

As membranas obtidas foram caracterizadas utilizando diversas técnicas de caracterização e os resultados sugerem que estas são adequadas para a utilização em engenharia de tecido ósseo, além disso, os ensaios de citotoxididade mostram queo novo agente reticulante é menos tóxico do que aqueles actualmente utilizados na literatura.

Palavras-chave: quitosano, ácido fítico, engenharia de tecidos

Abstract

Adult cartilage is very susceptible to lesions as time progresses due to its thickness, avascular nature and increased apoptosis. Aside from osteoarthritis being linked to the aging population, it is important to note that this kind of joint injuries happen frequently in the youth. Regardless of the cause, degeneration of articular cartilage can result in irreversible problems. Current treatment options are aggressive to the patient or still being developed.

With that in mind, it is of utmost importance to keep researching and find more viable solutions to help regenerate this type of tissue restoring it to its full capability.

The present invention discloses novel, stable and biodegradable membranes of proteins and/or polysaccharides, particularly of chitosan and chitosan/hyaluronic acid, useful as scaffolds for bone tissue engineering.

These membranes were fabricated by mixtures of polysaccharides and proteins of interest using novel crosslinking agents consisting of phytic acid (PA) derivatives obtained by a condensation reaction between phytic acid (PA) and a hydroxylic compound.

The membranes obtained were characterized using several characterization techniques and the results suggest that they are adequate for the utilization in bone tissue engineering, furthermore, the cytotoxicity assays showed that the novel crosslinking agent is less toxic than others currently being used in literature.

Keywords: chitosan, phytic acid, tissue engineering

Acknowledgments

First of all, I'd like to thank my parents for their patience and for offering me the opportunities I had during my education. Without their support I wouldn't have been able to achieve everything I have so far.

Professor Ana Leite for talking me into going to Madrid and all her support during and after my stay there.

My university professors that shared their knowledge and experiences during these years.

Dr. Julio San Roman, Drª Blanca Vasquez and Dr. Luiz Garcia for the patience and kindness demonstrated during this work, their help was priceless during my stay at their laboratory.

The people I met at Instituto de Ciencia e Tecnologia de Polímeros, they made me feel like at home.

And finally my friends, who always find a way to make me laugh and see the joy in life.

Table of Contents

Índice

List of Figures

List of Tables

Chapter 1 – Introduction

1.1 Chitosan

1.1.1 Chitosan molecular structure and properties

Chitosan is a copolymer prepared from chitin, which is the second most abundant natural polymer in nature after cellulose. Chitin is mostly obtained from the exoskeletons of arthropods like crustaceans and insects but other possible sources are krill, clams, oysters, and fungi and it has been estimated that more than 10 billion tons of chitin are biosynthesized each year (Zargar et al. 2015). Chitin is a linear polysaccharide composed of repeating units of poly β-(1→4)-N-acetyl-D-glucosamine (Fig. 1).

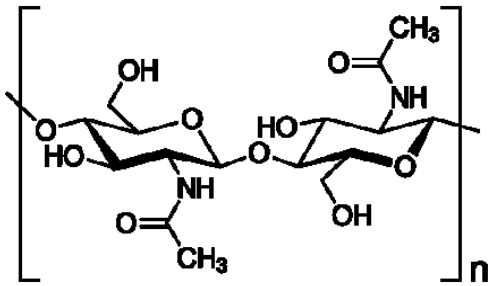

Figure 1 – Structure of the chitin molecule.

Chitin is bio-renewable, environmentally friendly, and it possesses several attractive properties such as biocompatibility, biodegradability and bio-functionality. Chitosan is a linear, natural copolymer composed of randomly distributed β-(1→4)-linked D-glucosamine and N-acetyl-D-glucosamine (NAG) units, whose molecular structure comprises a linear backbone linked through glycosidic bonds (Fig. 2).

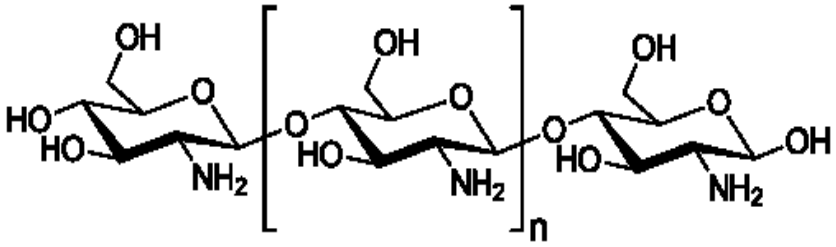

Figure 2 - Structure of the chitosan molecule.

Chitosan is obtained by deacetylation and depolymerisation of native chitin, partial deacetylation of chitin in the solid state under alkaline conditions, or enzymatic hydrolysis in the presence of a chitin deacetylase (Zargar et al. 2015). Thus, these polymers are essentially the same but with defined degrees of deacetylation (DD), which is the percentage of the deacetylated units present in the molecule chain.

Chitosan has several interesting properties that make it suitable for its use in the biomedical field such as biodegradability, abundance, biocompatibility and non-toxicity (Anitha et al. 2014; Kumar 2000; Kim et al. 2008). In contrast to chitin the presence of free amino groups ($-NH_2$) along the chitosan chain allows this macromolecule to dissolve in diluted aqueous acidic solvents due to the protonation of these groups, rendering the corresponding chitosan salt in solution ($-NH_3^+$) (Kumar 2000; Kim et al. 2008). This is one of the principal advantages of chitosan when compared with chitin, facilitating its handling in a wider range of applications ranging from fungicidal and water treatment to cosmetic, pharmaceutical and biomedical applications (Kumar 2000).

1.1.2 Chitosan as a biomaterial

As previously mentioned the presence of amine groups in chitosan makes that pH differences change its behaviour and properties. At low pH the amines protonate and chitosan is positively charged making it soluble in acidic media. Once the pH rises to above 6-6,5 the amine groups deprotonate, turning the chitosan insoluble (Dash et al. 2011). Another important characteristic that makes this polymer a very useful tool for tissue engineering is its biocompatibility which is due to chitosan's structure similarity with the mammalian glycosaminoglycans (GAGs), a polysaccharide present in the surface of cells and in the extra cellular matrix (ECM) (Dash et al. 2011).

Chitosan can be processed in several different ways. Nowadays it has been under research studies about chitosan nanoparticles, hydrogels, nanofibers and crosslinked membranes for application in bone tissue engineering, cartilage, liver, central nervous system and the development of drug and protein delivery systems and wound healing (Croisier & Jérôme 2013).

Considering the published studies and chitosan's excellent properties the membranes developed during this work are proposed as a possible solution for cartilage and subchondral bone lesions.

1.2 Phytic Acid

1.2.1 Phytic acid molecular structure and properties

Myoinositol hexaphosphate or phytic acid (PA) is a natural and ubiquitous antioxidant that constitutes 1-5 wt % of most cereals, nuts, legumes, and oil seeds (Graf & Eaton 1990). Its structure can be observed in Figure 3. PA has the ability to bind minerals, proteins and polysaccharides. However, despite the potential energy inherent in the six phosphoric ester linkages, phytic acid is very stable at neutral and alkaline pHs (Graf & Eaton 1990).

Figure 3 - Phytic Acid chemical structure

This biomaterial possesses a powerful antioxidant activity which is mainly due to its high affinity with polyvalent cations being able to form stable complexes with zinc, iron, calcium and magnesium, among others (Graf & Eaton 1990). As an antioxidant, PA is extraordinarily stable and its antioxidant activity is closely related with its high binding affinity for iron (Graf & Eaton 1990). By forming a unique iron chelate, it suppresses iron –catalyzed oxidative reactions in biological materials. In addition to this, other clinical advantages of PA are its anticancer effects and its ability to lower blood cholesterol and lipids (Ravichandran et al. 2013).

1.2.2 Phytic Acid as a biomaterial

In the biomedical field PA has already been used as a natural crosslinking agent of proteins and polysaccharides (Lee et al. 2011; Ravichandran et al. 2013). Cations of natural polymers can bind directly with anions of PA through electrostatic charges. Polysaccharides can also bind to PA via hydrogen bond formation. The advantages of PA against other multivalent non-toxic polyanions like tripolyphosphate (TPP) is that the number of anions capable of reacting with cations is two-fold higher than TPP (Oatway et al. 2001).

This work has been devoted to the synthesis of novel natural crosslinking agents based on phytic acid (PA) derivatives of condensates of PA with hydroxylic compounds, preferably glycerol. This type of natural crosslinking agent demonstrated to be useful in the preparation of stable biodegradable crosslinked gels of proteins and/or polysaccharides. The advantages of using the novel crosslinker respect to PA lie in its lower cytotoxicity and its higher compatibility with natural polymers. In addition, the crosslinked formulations provide antioxidant properties and ability to form complexes with polyvalent cations, of great importance in the regeneration processes of tissues.

1.3 Hyaluronic Acid

1.3.1 Hyaluronic acid molecular structure and properties

Hyaluronic acid (HA), also referred as hyaluronan is a ubiquitous non-sulfated glycosaminoglycan (GAG) present throughout the extracellular matrix of most connective tissues such as cartilage, vitreous of the eye, umbilical cord and synovial fluid (Falcone et al. 2006). HA may have several thousand sugar molecules in its chain, and when not bound to other molecules it binds to water giving it a stiff, viscous quality (Necas et al. 2008).

Commercially produced hyaluronic acid was previously extracted from either animal sources such like the vitreous bovine humor, synovial fluid, umbilical cord, skin and rooster crests or with the aid of bacteria like *Streptoccoccus sooepidemicus* and *Streptoccoccus equi* through fermentation or direct isolation. The improvement of this isolation processes resulted in the commercial availability of numerous molecular weight grades (Liu et al. 2011). Several of HA's fundamental physicochemical properties are dependent on its molecular weight, thus the distinct differences in function of the wide range of commercially available molecular weights enables HA to be used in a diverse set of applications. Additionally, chemical modification can provide a more mechanically and chemically stable biomaterial while retaining its biocompatibility and biodegradability expanding its range of applications (Liao et al. 2005).

Hyaluronic acid is composed of disaccharide repeating units of D-glucuronic acid (GlcUA) and N-acetylglucosamine (GlcNAc) joined alternately by β-1, 3 and β -1, 4 glycosidic bonds. This chemical structure can be observed in Figure 4.

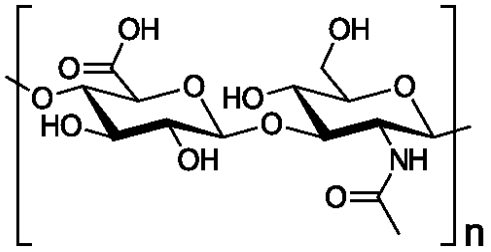

Figure 4- Hyaluronic Acid repeating unit.

Hyaluronic acid is biocompatible, biodegradable, anti-inflammatory, non-immunogenic and non-thrombogenic. In cartilage, HA binds aggrecan to form large aggregates within the collagenous framework, providing compressive resistance to the tissue. Cellular interactions between chondrocytes and HA help organize the cartilage ECM and retain the proteoglycans within the cartilage (Kuettner 1992). Natural HA can be easily degraded by natural enzymes such as hyaluronidase. However, chemical modification and covalent crosslinking helps stabilize HA while improving its properties (Falcone et al. 2006).

During this work, it was used sodium hyaluronate, which is HA in the form of sodium salt. Sodium hyaluronate has the same properties of HA and their chemical structure are very similar (Fig. 5). It can be observed that in the GlcUA unit there is a sodium carboxylate group instead of a carboxyl.

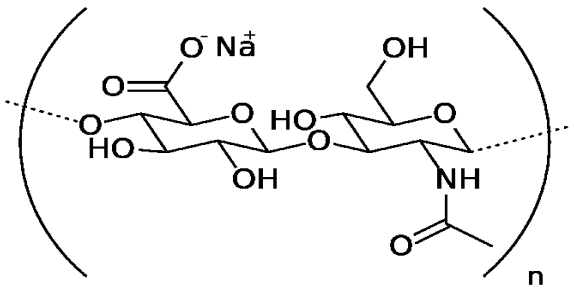

Figure 5 - Sodium hyaluronate chemical structure

1.3.2 Hyaluronic acid as a biomaterial

Due to the intrinsic biocompatibility of HA, this biomaterial is currently used in a wide variety of biomedical applications such as the synthesis of membranes for tissue engineering and production of hydrogels, and in the treatment of the inflammatory process in medical areas such as orthopaedics, dermatology and ophthalmology (Necas et al. 2008).

Being present in high concentrations in the skin and soft tissues makes it an appropriate choice for a matrix to support dermal regeneration. Studies have shown that biomaterial surfaces treated with cross-linked HA have been associated with reduced platelet adhesion and thrombus formation making HA an effective choice for decreasing the risk of infections in cardiovascular implants. More importantly HA plays a very important role in cartilage development, the maintenance of synovial fluid and the regeneration of tendons (Necas et al. 2008). Partly due to its viscoelastic nature and ability to form highly hydrated matrices, HA acts in the joint as a lubricant and shock absorber (Leach et al. 2004). The most relevant properties for the use of HA as a biomaterial in biomedical applications are summarized in Fig. 6.

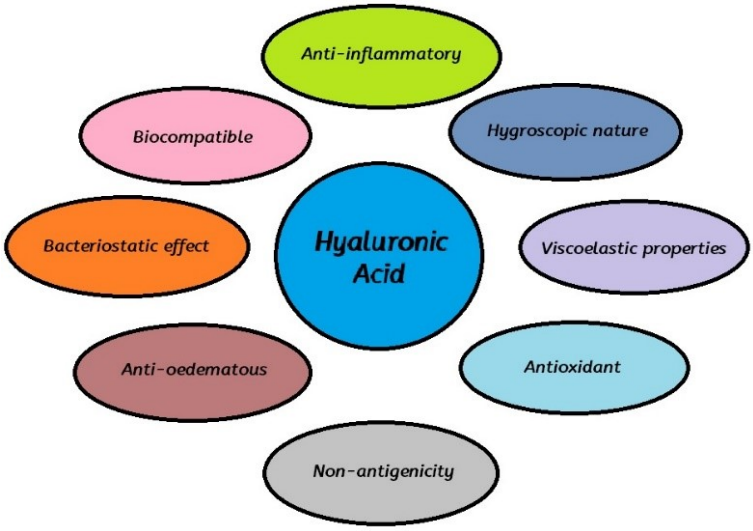

Figure 6- Summarized properties of Hyaluronic Acid

1.4 Osteochondral tissue structure: Articular Cartilage, Subchondral Bone and their associated pathologies

1.4.1 Articular Cartilage and Subchondral Bone

The tissues that form and support joint surfaces are in general called osteochondral tissues. The most superficial of these is the articular cartilage which is a specialized tissue that plays a very important role in the natural joints because it increases joint consistency, protects the subchondral bone from high stresses and reduces friction at the edge of long bones (Panseri et al. 2012).

Healthy articular cartilage is mainly composed of a dense extracellular matrix (ECM) of collagen organized in fibrils and a small percentage of chondrocytes.

Unlike other self-repairing tissues, articular cartilage doesn't possess a vascular, neural or lymphatic network nor local progenitor cells, it is nourished by the synovial fluid that irrigates its surface and, to a lesser extent, by the diffusion of blood substrates from the subchondral bone blood vessels, which explains why it is so difficult to restore damaged or diseased articular cartilage (Zhang et al. 2009).

This type of cartilage is divided into four different zones according to the composition and organization of the cells and ECM molecules, the different proportions of the components present in the ECM influence the mechanical properties of each area (Nooeaid et al. 2012). These are referred as the superficial tangential zone (STZ), middle (or transitional), deep (or radial) and calcified zones (Zhang et al. 2009).

The STZ composes approximately 10% to 20% of articular cartilage thickness. It contains a high number of flattened chondrocytes and possesses collagen fibbers (mostly type II and IX collagen) grouped firmly and parallel to the surface. This zone integrity is of utmost importance due to its function of protection and maintenance of deeper layers. The middle (transitional zone) represents 40% to 60% of the total cartilage and serves has an anatomic and functional link between the superficial and deep zones. This zone has proteoglycans; the collagen fibrils are organized obliquely and the chondrocytes are spherical and at low density.

The deep zone collagen represents 30% to 40% of the articular cartilage volume and its fibrils are organized perpendicular to the articular surface, it has the highest proteoglycan content and the lowest water concentration, making this zone the responsible for providing the

greatest resistance to compressive forces (Sophia Fox et al. 2009). The chondrocytes are frequently arranged parallel to the collagen fibbers and perpendicular to the joint line. The tidemark discerns the deep zone from the calcified cartilage. This calcified cartilage connects the articular cartilage to the subchondral bone by anchoring its collagen fibrils to the subchondral bone (Sophia Fox et al. 2009). In this zone the cell population is limited and the chondrocytes are hypertrophic.

The subchondral bone is the subarticular mineralized tissue that extends from calcified cartilage to the beginning of the bone marrow. Its main functions are to support the overlying joint cartilage, distribute the mechanical load on the underlying cortical diaphysis, absorb the continuous tension of the mechanical impacts and nourish the deeper layers of articular cartilage, especially during the growth period. Despite subchondral bone anatomy being very variable it can be anatomically divided into two distinct areas: the subchondral bone plate (SBP) and the subchondral trabecular bone (STB) (Li et al. 2013). The SBP is a thin cortical layer in contact with the calcified cartilage, its high porosity allows several arterial, blood vessels and nerves creating a bridge between articular cartilage and the STB (Madry et al. 2010). Some factors such as age or the magnitude of the compressive forces affect the distribution and intensity of this channels. The line which separates the calcified zone from the subchondral bone plate is called “cement line”. Arising from the subchondral bone plate is the supporting trabeculae, which is composed by the STB and deeper bone structure. The subchondral trabecular bone has a very important role as a shock-absorber and support in normal joints. When compared to the SBP, it is more porous and metabolically active due to the presence of a vascular network, sensory nerves and bone marrow (Li et al. 2013)

1.4.2 Cartilage defects and current treatments

Adult cartilage is very susceptible to lesions as time progresses do to its thickness, avascular nature and increased apoptosis. Moreover, menopause, diabetes and anti-inflammatory treatments have been shown to negatively influence cartilage properties (Nukavarapu & Dorcemus 2013). Cartilage injuries are classified as osteochondral defects, chondral defects, and cartilage microfractures. Within the range of cartilage lesions the least harmful type are microfractures, but even though the immediate impact to the matrix is not visible to the naked eye, this kind of lesion alters its load distribution leading to the thickening of the calcified layer and subchondral bone and subsequent thinning of the articular cartilage, this type of lesion also damages the collagen network effecting superficial GAG loss (Athanasiou et al. 2009). Chondral defects can be characterized in two different ways: partial chondral defects when only the articular cartilage is damaged or full thickness defect where the damage is spread to the subchondral bone. Chondral defects can proceed from cartilage microfractures or trauma, improper loading, or foreign bodies. With its avascular nature, the intrinsic metabolic activity is insufficient to result in an adequate repair which leads to the eventual development of osteochondral fissures. Osteochondral defects are defined by the exposure of the subchondral bone (Madry et al. 2010). Additionally, lesions involving both the articular cartilage and the subchondral bone lead to the formation of fibrocartilage that has different biomechanical properties from the native articular cartilage and does not protect the subchondral bone from further degeneration (Panseri et al. 2012). Regardless of the cause, degeneration of articular cartilage can result in irreversible problems, such like osteoarthritis (L. Radin 2004). During the past two decades, several cartilage reparative and restorative procedures have been developed. The current therapeutic tools aim to fill the cartilage loss to restore joint congruence, inducing hyaline healing and thus preventing long-term osteoarthritic degeneration (Montgomery et al. 2014).

Current options for the treatment of this kind of injuries include microfractures, debridement, osteochondral autograft and allograft transplants, subchondral marrow stimulation, and regeneration via autologous chondrocyte cells implantation (Versier & Dubrana 2011; Camp et al. 2014). Second-generation systems are also available; these use absorbable scaffolds to support autologous chondrocytes prior to implantation.

Aside from OA being linked to the aging population, it is important to note that this kind of joint injuries happen frequently in the youth, furthermore osteochondrosis and osteochondritis dissecans are joint diseases that occur mainly to children, due to the vulnerability to stress in the growing skeleton (Athanasiou et al. 2009). It is of utmost importance to keep researching and find more viable solutions to help regenerate this type of tissue restoring it to its full capability.

Chapter 2 - Hypothesis and Objectives

Due to the great interest in developing new biomedical applications using chitosan, the main objective of this work has been the production and study of the behaviour of membranes based on hydrogels of chitosan crosslinked with sodium hyaluronate utilizing a novel crosslinking agent, a product from the reaction between phytic acid and glycerol (GPhy).

In this sense, this work was focused in three specific aims:

- Successfully carry out the chemical reaction between glycerol and phytic acid and subsequent study of its final product;

- Successfully produce Ch membranes crosslinked with GPhy and study its characteristics;

- Successfully produce Ch/HA membranes crosslinked with GPhy and study its characteristics.

Chapter 3 - Material and Methods

3.1 Chitosan purification

For this laboratory work two different types of chitosan were used, a Ch of medical grade supplied by Altakin, Portugal and another provided by IDEBIO, Spain. Due to the large content of impurities in IDEBIO's chitosan it had to be purified prior to utilization. At first, the chitosan (5 g) was dissolved in a solution (0.5 % w) of glacial acetic acid (0.5 M) at room temperature and under continuous stirring during 24 h. Once this time had passed the solution was heated at 50 ºC for 30 min and then vacuum filtered using conventional filter paper. The filtered solution was then neutralized by addition of NaOH (1 M) until pH = 8. At this pH value the chitosan starts to precipitate do to its soluble-insoluble transition at pH 6 – 6,5 (Dash et al. 2011). Once the chitosan was completely precipitated a second filtration process was started to remove the supernatant. The chitosan was then repeatedly washed with a blend of water and ethanol with different concentrations (v/v), 1:9, 3:7, 1:1, 2:1 using a centrifuge at 8000 rpm for 8 minutes at a temperature of 5 ºC for each wash. The washed chitosan was placed in vials and stored at -72 ºC for 24 hours. Once this period was over the chitosan was lyophilized for 48 h to remove all its water content. At the end of this process a light, spongy mass was obtained and grinded into a fine powder.

3.2 Synthesis and characterization of PA derivative crosslinkers: Glycerol Phytate (GPhy)

3.2.1 First GPhy synthesis

For this synthesis, it was used glycerol and phytic acid sodium salt from Sigma-Aldrich. The synthesis of GPhy was carried out in bulk in acidic pH, using a PA:G mass ratio of 1:1 and at a temperature of 120ºC.The reaction was allowed to proceed for 12 h.

Afterwards, the reaction product was dissolved in water and precipitated in acetone.The precipitate was dissolved in 0.1 M NaOH and reprecipitated in acetone. The mixture was kept in the fridge for 12 h and the product filtered, dissolved in a minimum amount of water, and lyophilized. The GPhy obtained was liquid at room temperature and stored in the refrigerator.

3.2.2 Second GPhy synthesis

For this synthesis, it was used glycerol and phytic acid sodium salt from Sigma-Aldrich. The synthesis of GPhy was carried out in bulk, using a PA:G molar ratios in PA:G molar ratio of 1:7 and at a temperature of 120ºC. The reaction was allowed to proceed for 12 h under mechanical stirring. Afterwards, the reaction product was dissolved in water and precipitated in 2-propanol. The isolated product was dissolved in a minimum amount of water, and lyophilized. The GPhy crosslinker was stored in the refrigerator.

3.3 Preparation of Ch membranes crosslinked with the first GPhy synthesis

Purified Ch from IDEBIO was dissolved (2 wt-%) in 0.25 wt-% acetic acid solution. Then, the corresponding amount of GPhy was added. The mixture was stirred for 15 min and then ultrasonicated, and then placed into a Teflon mould, transferred to an oven at 37 ºC and kept there until complete evaporation of the solvent. The hydrogel membrane was removed from the mould, washed with 1 M NaOH and then with distilled water until neutral pH. The membrane was then dried at 37 ºC. The names and composition of Ch hydrogel membranes prepared with different proportions of GPhy are reported in table 1.

Table 1 - Composition of the Ch hydrogel membranes crosslinked with GPhy.

Sample name	GPhy (wt-% respect to Ch)
QGPhy2.5	2.5
QGPhy5	5
QGPhy10	10

3.4 Preparation of Ch/HA membranes crosslinked with the first GPhy synthesis

For the synthesis of this membranes it was used sodium hyaluronate from BIOIBERICA with M_w=1000 kDA. Purified Ch from IDEBIO was dissolved (2 wt-%) in 0.25 wt-% acetic acid solution. Separately, HA was dissolved (2 wt-%) in aqueous solution. Aliquots of both solutions were mixed under agitation and 50 µl of 1 N HCl were added to obtain complete solution of both polysaccharides. Then, the corresponding amount of GPhy was added The mixture was vigorously stirred for 15 min, ultrasonicated, place into a Teflon mould, transferred to an oven at 37ºC and kept there until complete evaporation of the solvent. The hydrogel membrane was removed form the mould, washed with 1 M NaOH and then, with distilled water until neutral pH. The membrane was then dried at 37ºC. Hydrogel membranes with Ch/HA mass ratios reported in table 2 were prepared.

Table 2 - Names and composition of the Ch/HA formulations used for the preparation of hydrogel membranes crosslinked with GPhy.

Sample name	Ch/HA (wt/wt)	GPhy (% respect to Ch)
6:4QHA2.5	60:40	2.5
6:4QHA5	60:40	5
6:4QHA10	60:40	10

3.5 Preparation of Ch membranes crosslinked with the second GPhy synthesis

Altakin's Ch was dissolved (2 wt-%) in 0.25 wt-% acetic acid solution. The mixture was stirred for 15 min and then ultrasonicated, and then placed into a Teflon mould, transferred to an oven at 37 ºC and kept there until complete evaporation of the solvent. The hydrogel membrane was removed from the mould, washed with 1 N NaOH and then with distilled water until neutral pH. The obtained Ch membrane was immersed in 10 mL of an aqueous solution of GPhy (2.5, 5, 10 or 50 wt % in different experiments) and kept overnight at 37 º C. Then, the corresponding crosslinked membrane was washed with distilled water and dried. The names and composition of Ch hydrogel membranes prepared with different proportions of GPhy are reported in table 3.

Table 3 - Composition of the Ch hydrogel membranes crosslinked with GPhy.

Sample name	GPhy (wt-% respect to Ch)
ChGPhy2.5	2.5
ChGPhy5	5
ChGPhy10	10
ChGPhy50	50

3.6 Preparation of Ch/HA membranes crosslinked with the second GPhy synthesis

For the synthesis of this membranes it was used sodium hyaluronate from BIOIBERICA with M_w=1000 kDA. Altakin's Ch was dissolved (2 wt-%) in 0.25 wt-% acetic acid solution. Separately, HA was dissolved (2 wt-%) in aqueous solution. Aliquots of both solutions were mixed under agitation (Ch/HA mass ratio of 60:40) and slightly acidified with 1 N HCl to obtain a complete solution of both polyssacharides which was ultrasonicated, placed into a Teflon mould, transferred to an oven at 37ºC and kept there until complete evaporation of the solvent. The membrane was crosslinked by immersion in GPhy solutions (2.5, 5 and 10 wt-% in respect to Ch, in different experiments) for 12 h at 37º C. The corresponding hydrogel membrane was removed from the mold, washed with 1 N NaOH and distilled water until neutral pH. The membrane was then dried at 37 º C.

Table 4 - Names and composition of the Ch/HA formulations used for the preparation of hydrogel membranes crosslinked with GPhy.

Sample name	Ch/HA (wt/wt)	GPhy (% respect to Ch)
6:4ChHA2.5	60:40	2.5
6:4ChHA5	60:40	5
6:4ChHA10	60:40	10

3.7 Characterization techniques

3.7.1 Nuclear Magnetic Resonance

During this experiment proton (^{1}H-NMR), carbon 13 (^{13}C-NMR) and phosphorous 31 (^{31}P-NMR) nuclear magnetic resonance spectra were obtained for different samples using a Bruker Avance-300 (Fig.7) spectrometer.

Figure 7 - Bruker Advance - 300 spectrometer.

The preparation of each sample was done accordingly to the wanted spectrum and the sample itself. For the ^{1}H-NMR spectra, 20 mg of each sample was introduced into different NMR tubes together with 1 mL of deuterated water (D_2O). For the specific case of chitosan, it was prepared a solution of 35%w deuterated hydrochloric acid (DCl) in D_2O, thus obtaining a final dissolution of 0.5%w. Then, 20 mg of chitosan was added to 1mL of this dissolution and left stirring until homogeneous. For the GPhy and Glycerol, dimethyl sulfoxide (DMSO) was utilized instead of D_2O. For the ^{13}C-NMR spectra, approximately 50 mg of sample was added to 1 mL of D_2O. For PA, Glycerol and PA derivative it was used DMSO together with 30 microliters of phosphoric acid instead of D_2O.

3.7.2 Fourier transform infrared spectroscopy - Attenuated total reflectance (FTIR-ATR)

FTIR-ATR spectrums were obtained with the aid of a Perkin-Elmer Spectrum 1 spectrometer (Fig. 8). Samples of non-purified chitosan, purified chitosan, glycerol, phytic acid, non-purified glycerol phytate, purified glycerol phytate, Ch and Ch/HA membranes crosslinked with GPhy were analyzed.

Figure 8 - Perkin-Elmer Spectrum 1 spectrometer

3.7.3 Thermogravimetric analysis (TGA)

The thermic degradation of all samples was analyzed with the aid of TA Instrument's TGA Q500 (Fig. 9). The temperature ranged between 40 º C and 800 º C at a heating rate of 10 ºC/min using a nitrogen atmosphere. From the corresponding TGA thermograms it was possible to obtain the temperatures in which the weight losses were 5% ($T_{5\%}$) and 50% ($T_{50\%}$), and the final corresponding residue. From the derivative curve (DTGA) it was possible to obtain the temperature at which the degradation velocity was at its maximum (T_{max}). Samples of purified and non-purified Ch, HA, PA, glycerol, GPhy, Ch and Ch/HA membranes crosslinked with GPhy were analyzed.

Figure 9 – TA Instrument's TGA Q500

3.7.4 Scanning Electron Microscopy (SEM)

The scanning electron microscopy images were obtained using a Hitachi SU8000 (Fig. 10). Samples of Ch membranes and Ch/HA crosslinked with GPhy were analyzed.

Figure 10 - Hitachi SU8000

3.4.5 Differential Scanning Calorimetry (DSC)

Differential scanning calorimetry experiments were carried out on a micro-DSC-Illa (Setaram, France). Three heating-cooling cycles were analyzed between 25ºC and 180ºC with a scanning rate of 10ºC/min under nitrogen at 20 mL/min flow rate. Standard Hastelloy vessels were used with 3 mg sample weight approximately. Empty vessel was used as reference. From the thermograms, the glass transition temperature was determined as the midpoint of the transition.

3.8 Swelling behavior

Swelling experiments were performed in PBS of pH = 7.4 at 37 °C. The corresponding sample was immersed in 5 mL of the medium and kept under static conditions. The sample was removed at appropriate times and dried rapidly with filter paper for removing excess water on the surface and, thus weighed. The percentage of the water uptake was calculated by eq. (1), where w_t is the weight of the sample at time t and w_d is the initial (dry) weight of the sample.

$$Water\ \ uptake\ \ (\%) = \frac{w_t - w_d}{w_d} x100 \qquad \text{eq. (1)}$$

In all the experiments, a minimum of four samples of each composition were measured and results averaged. Statistical analysis (ANOVA) of results at different times for each sample was performed with respect to time of maximum water uptake value at a significance level of 0.05 (*p<0.05 respect to t = 1 day and #p<0.05 respect to t = 2 days).

3.9 Determination of free amino groups

The determination of the free amino groups was done by potentiometric titration. This analysis was made to the purified chitosan and the membranes done during this laboratorial work. First, it was prepared a 0,1 M chloridric acid (HCl) solution to which 0,2 g of the sample was added in a magnetic stirrer for 24 hours to achieve the protonation of the present amino groups.

The resulting solution was then titrated with NaOH (0.096 M) previously normalized with potassium phthalate. The pH was measured as NaOH was added to obtain a curve where two characteristic volumes were obtained. Finally, equation (2) was used to calculate the free amino groups.

$$\%NH2 = \left[MNaOH(V2 - V1)\ \times \frac{161}{m}\right] \qquad \text{eq. (2)}$$

Where $\%NH_2$ is the percentage of free amino groups in the sample, M_{NaOH} the molarity of the NaOH dissolution, V_2 the volume of NaOH solution necessary to neutralize the excess of protonated amino groups and V_1 the volume of NaOH dissolution necessary to neutralize the excess of HCl. The number 161 corresponds to the molecular weight of the glucosamine unit of chitosan and m is the mass of the sample before titration.

3.10 Determination of deacetylation degree

The determination of chitosan's deacetylation degree (%DD) was done from its ^{1}H-NMR spectrum. Once obtained, the integrals corresponding to the acetyl group protons and to the C_2 proton of N-glucosamine unit were calculated. The equation (3) was used to obtain the deacetylation degree. In order to carry out the calculations, it was taken into account that the chitosan's acetyl group has three protons and therefore the integral of this signal has to be divided by 3.

$$\%DD = \left[1 - \frac{\int Hacetyl}{\int H(2-Nglucosamine)}\right] = \left[1 - \frac{\frac{H(2ppm)}{3}}{H(3ppm)}\right] \quad \text{eq. (3)}$$

3.11 Mineralization assays

Apatite layer growth was studied on membranes after immersion in SBF1.5 medium prepared according to reference (Oliveira et al. 2015).The morphology of the surface at different times of immersion in SBF.15 was examined by SEM and by EDX using a Hitachi SU8000 FE-SEM apparatus at an accelerating voltage of 25 kV. Energy dispersive X-rays (EDX) analyzer Bruker XFlash model with detector 5030 was used. The composition of the surface was analysed by ATR-FTIR spectroscopy.

3.12 Biological assays

Cellular toxicity was evaluated using fibroblast of human embryonic skin (HFB, Innoprot). Cells were cultured in Dulbecco's modified Eagle's medium (DMEM) supplemented with HEPES (for HFB cells) and 10% fetal bovine serum (FBS), 100 units mL^{-1} penicillin, 100 μg mL^{-1} streptomycin and 200 mM L-glutamine. A humidified atmosphere at 37 °C with 5% CO_2 and 95% of air was used for cell cultures growth. For cell experiments, cells were harvested using 0.25% trypsin and 1 mM EDTA in Hanks buffer.

3.12.1 Cytotoxicity of GPhy crosslinkers

The evaluation of cytotoxicity of PA, GPhy and commercial β-GP was determined by MTT assay. A stock solution of the corresponding sample in DMEM was prepared and successive dilutions were tested. Cells were seeded at a density of 9 x 10^5 cells/mL in complete medium and incubated to confluence. After 24 h of incubation the medium was replaced with the corresponding dilution and incubated at 37 ºC in humidified air with 5 % CO_2 for 24 h. A solution of MTT was prepared in warm PBS (0.5 mg/mL) and the plates were incubated at 37ºC for 3 h. Excess medium and MTT were removed and 100 μL DMSO were added to all wells. This was mixed for 10 min and the absorbance was measured with a Biotek SYNERGY HT Plate Reader using a test wavelength of 570 nm and a reference wavelength of 630 nm. The percentage of relative cell viability (CV) was calculated from eq (4):

$$CV\ (\%) = 100 \times (OD_S - OD_B)/(OD_C - OD_B) \qquad \text{eq (4)}$$

Where OD_S, OD_B and OD_C are the optical density of formazan production for the sample, blank and control respectively. A dose-response curve of relative cell viability was plotted to delineate the concentrations of the tested sample that depressed MTT-formazan production by 50% (IC_{50} value).

3.12.2 Cytotoxicity of crosslinked polysaccharide membranes

The evaluation of cytotoxicity of membranes was determined by MTT assay. The corresponding sample was set in FBS-free DMEM. Then, extracts of the medium were removed at different time periods (1, 2, 7 and 14 days) and replaced with fresh medium. The extracts were filtered and used for cytotoxicity assays. Thermanox® (TMX) discs were used as negative control. Separately, cells were seeded at a density of 9 x 10^4 cells/mL in complete medium, and incubated to confluence. After 24 h of incubation the medium was replaced with the corresponding extract and incubated at 37 ºC in humidified air with 5 % CO_2 for 24 h. The rest of the test was carried out as explained above.

Analysis of variance (ANOVA) of the results for tested materials was performed with respect to control at significance level of *$p<0.05$.

3.12.3 Cellular morphology

The materials were placed in a 24-well plate (in duplicate), seeded with cells at a density of 5 x 10^4 cells/mL and incubated at 37 °C. After 24 h, 4, and 8 days incubation periods, the cells were fixed with 2.5% glutaraldehyde buffered in 0.1M PBS. The dried samples were examined under a scanning electron microscopy (SEM) using a Philips XL 30 apparatus at an accelerating voltage of 15 keV.

Chapter 4 - Results and Discussion

Part I

In this part of the laboratory procedure, it was used the chitosan provided by IDEBIO after its purification process and the GPhy obtained from the first synthesis as described in subchapter 3.2.1. All results presented in this subchapter were obtained using chitosan from IDEBIO and the first synthesis of GPhy.

4.1 Synthesis and characterization of GPhy

The crosslinking agent GPhy was synthesized by a condensation reaction between G and PA. The purified GPhy was characterized by FTIR spectroscopy along with its precursors, G and PA. The ATR-FTIR spectrum of GPhy (Fig. 11) showed the main representative bands present in the spectra of both precursors. They are as follows: a broad band at 3248 cm^{-1} due to stretching vibrations of O-H groups, bands at 2943 and 2888 cm^{-1} due to asymmetric and symmetric vibrations of C-H bonds of the inositol ring. At lower wavenumber, the spectrum showed a band at 1453 cm^{-1} due to deformation vibrations of C-H bonds of the inositol ring and G residues, a shoulder at 1187 cm^{-1} attributed to P=O stretching vibrations, a broad band centred at 1036 cm^{-1} due to stretching vibrations of C-O, P-O bonds present in the structure of phytate and G residues but also to stretching of P-O-C bonds formed in the condensate and a band at 918 cm^{-1} attributed to stretching of P-O and P-O-C bonds. This assignment was realized taking into consideration the study of Ishiguro (Ishiguro et al. 2003) carried out by different phytate samples.

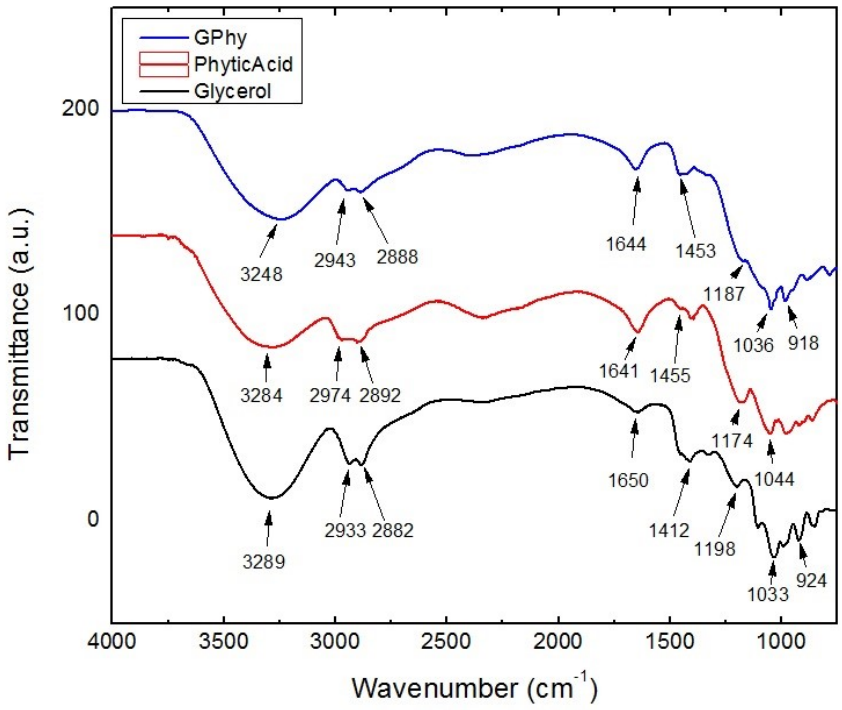

Figure 11 - GPhy, PA and G ATR-FTIR spectra.

GPhy was analysed by NMR. The ^{1}H NMR spectrum of GPhy (Fig. 12) showed signals belonging to precursors and additional signals due to the formation of the condensate. At lower chemical shift one multiplet signal appear between 3.42 and 3.74 ppm that can be assigned to $^{1}CH_2$-, $^{2}CH_2$ and CH protons of G according to assignment reported in literature (Govindaraju et al. 2000). These bands appear less resolved than in the spectrum of initial G in which two doublet-of-doublet between 3.45 ppm and 3.60 ppm (CH_2 protons) and a multiplet signal between 3.65 and 3.73 ppm (CH protons) were observed. At higher chemical shift, three small and broad signals between 4.15 and 4.6 ppm can be assigned to the PA protons in the GPhy: the signal at lower field is assigned to proton H_6 and the rest of signals that appear between 4.1 and 4.45 ppm are assigned to protons H_1-H_5 (Crimella et al. 1992). In addition, in the spectrum of GPhy a new multiplet signal between 3.76 and 3.90 ppm and a new triplet signal between 3.96-4.02 ppm appear that can be tentatively assigned to G protons that have reacted with PA (CH_2-O-P and CH-O-P). For comparison purposes, the ^{1}H NMR spectrum of β-G phosphate (GP) (Fig. 13) was recorded. In fact, this spectrum showed a signal between 3.50-3.70 ppm that can be assigned to the CH_2 protons of G moiety and a multiplet between 4.05-4.15 ppm that can be attributed to the resonance of CH-O-PO_3Na_2 protons.

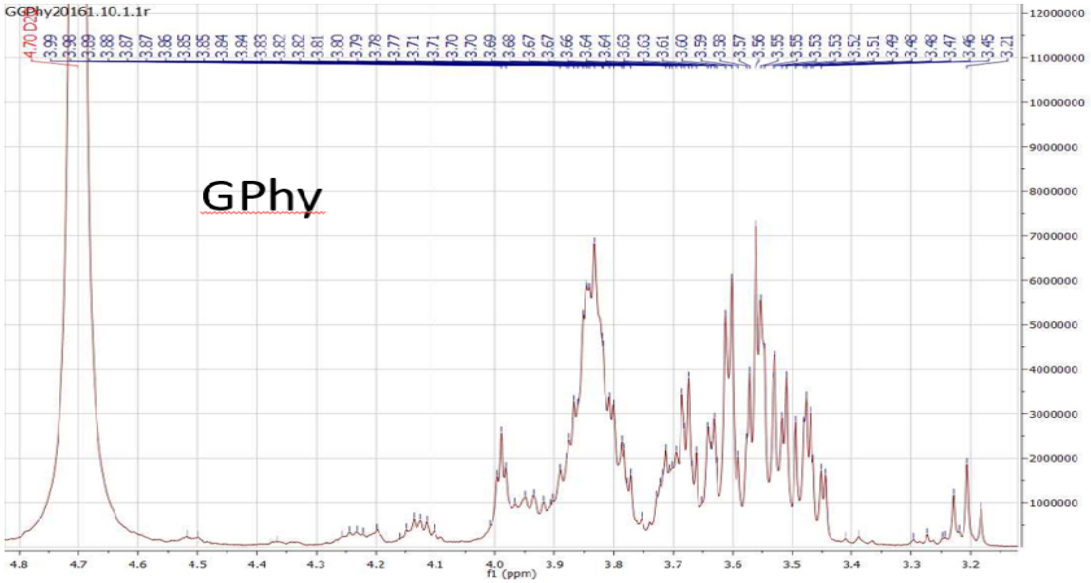

Figure 12 - GPhy ^{1}H NMR spectrum

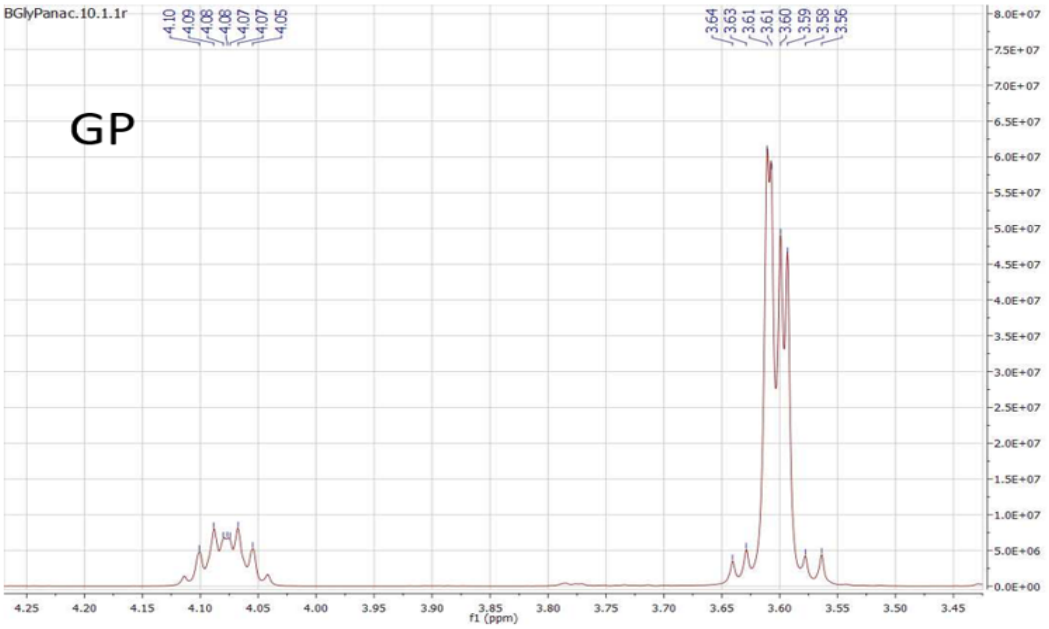

Figure 13 - β-G phosphate ^{1}H NMR spectrum

The elemental analysis results can be observed in table 5, GPhy gave a C/H ratio of 3.9 and this value was in between of those obtained for G (C/H =4.2) and PA (C/H=3.3). This result reflects the obtaining of the novel condensate by reaction of G with PA.

Table 5 - G, Pa and GPhy Elemental analysis results.

Samples	%C	%H	%N	C/N
G	37.5	8.9	0.1	4.2
PA	8.5	2.6	0.1	3.3
GPhy	18.0	4.6	0.1	3.9

Thermal degradation of GPhy was studied by TGA taking into consideration that of precursors and that of β-GP. Thermogravimetric (TGA) and differential thermogravimetric (DTGA) curves are shown in Fig. 14-16. Weight loss of GPhy underwent in four steps giving the respective maxima in the DTGA curve. The first one with T_{max} around 115ºC can be attributed to the loss of water contained in the sample. Then, one degradation step with maximum rate at 220ºC would involve the degradation of the G rest (T_{max}=218ºC) and part of the phytate rest (T_{max}=220ºC) by comparison with the TGA curves of the precursors. The degradation steps with maximum rates at 310ºC and around 450ºC (broad maximum) would correspond to the rest of the degradation of the phytate moiety. However, the T_{max} (450ºC) of the fourth degradation step notably increased with respect to that of PA (T_{max} =375ºC) indicating a higher thermal stability of the condensate tentatively attributed to the presence of the C-O-P-O-C bonds. The residue of GPhy was 54%. This value was notably reduced with respect to that of PA, indicating the content of G, which gives no residue at all. The thermal degradation patterns of GPhy and β-GP showed a great similitude, although the thermal stability of GPhy was higher than that of β-GP. TGA results of all the materials analysed are summarized in table 6.

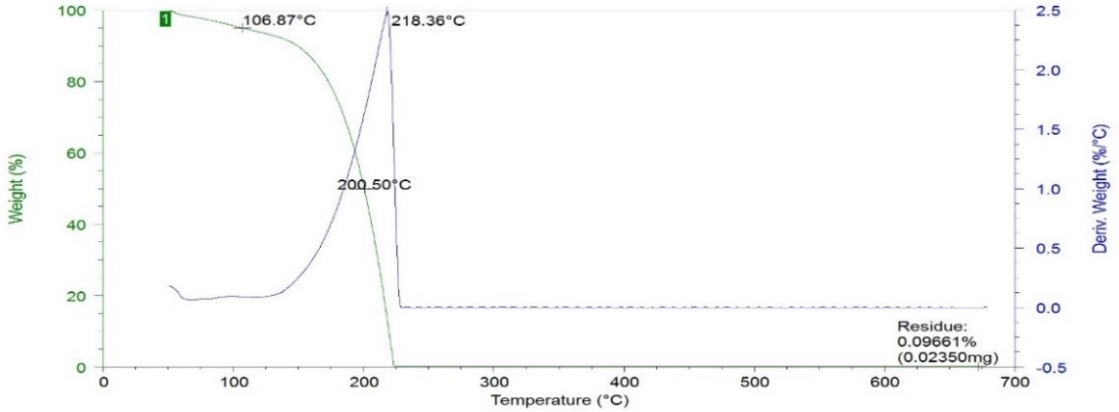

Figure 14 - Glycerol TGA results.

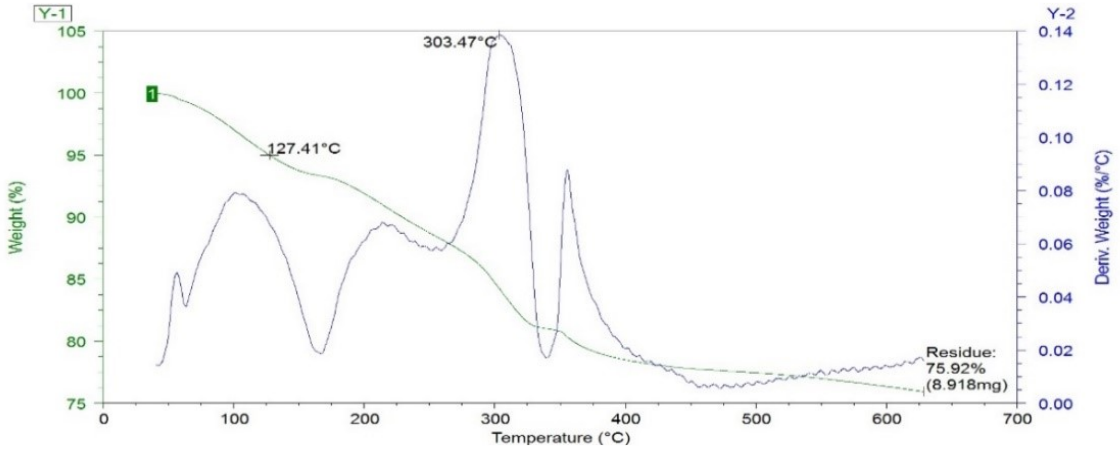

Figure 15 - Phytic Acid TGA results.

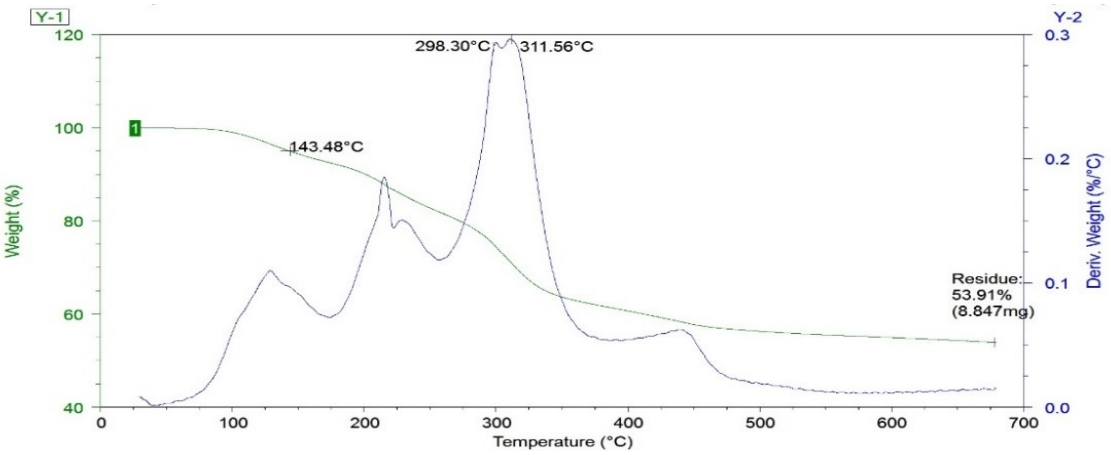

Figure 16 - GPhy TGA results.

Table 6 - Thermal degradation results of GPhy, their precursors and β-GP.

Sample	T_{max} (°C)				Residue (%)
	1st stage	2nd stage	3rd stage	4th stage	
G	218	-	-	-	0
PA	100	220	303	375	76
GPhy	115	220	310	450	54
β-GP	96	275	350	-	47

Cytotoxicity of GPhy was tested against human fibroblasts along with those of PA and β-GP. Fig. 17 shows the dose–response curves of relative cell viability for each compound. From the linear portions of the curves, the IC_{50} values were determined as the concentration that depressed MTT–formazan production by 50%. Values of IC_{50} for PA, GPhy and β-GP were 7.91 ± 0.05 mg/ml, 9.77 ± 0.10 mg/ml and 9.30 ± 0.03 mg/ml respectively, showing that GPhy and β-GP were less cytotoxic than PA against fibroblasts. Cytotoxicity of GPhy was comparable to that of β-GP.

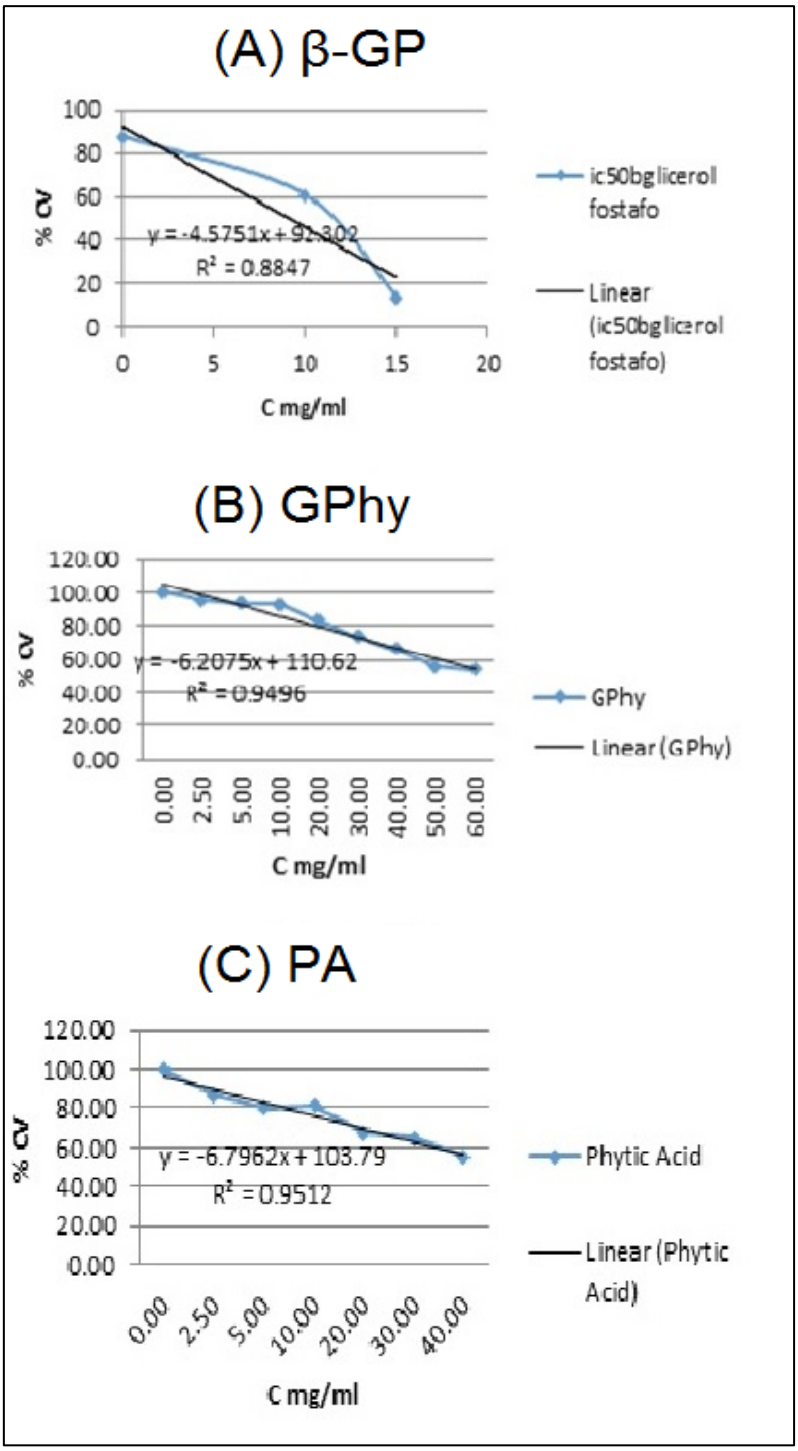

Figure 17- Dose-response curves of relative cell viability for (A) β-GP, (B) GPhy and (C) PA.

4.2 Chitosan purification and characterization

First of all, a chitosan purification was performed by following the protocol described in subchapter 3.1. The chitosan characterization was carried out once the purification process was finished. It's possible to verify in Fig. 18 that there are macroscopic differences between the unpurified chitosan and purified chitosan samples.

Figure 18- Impure chitosan (left) and purified chitosan (right).

The purified chitosan was characterized by NMR. With the ^{1}H-NMR spectrum in deuterated hydrochloric acid (0,5%w) obtained (Fig. 19) it was possible to determine its deacetylation degree. In this spectrum it is highlighted the signal corresponding to the protons of the acetyl groups at 2.3 ppm and the signal from the proton bound to the C_2 of the glucosamine unit at 3.4 ppm. Between 3.8 and 4.2 ppm the signals from all other protons can be observed except for the proton signal of the anomeric carbon which is at 5.2 ppm. The peaks corresponding to the protons of the acetyl group and the C_2 proton of the N-glucosamine unit were utilized for the deacetylation degree calculation. The values obtained for the integrals of each peak were used in equation (3) and are shown in Table 7 together with the theoretical deacetylation degree provided by the supplier and the deacetylation degree calculated by this method.

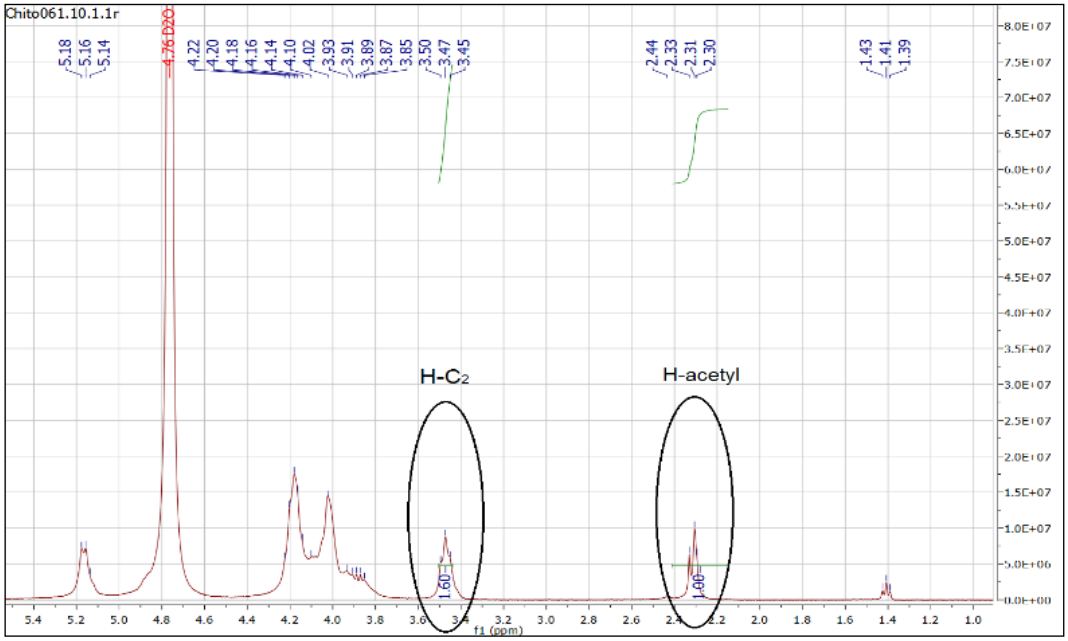

Figure 19- [1]H-NMR purified chitosan spectrum

Table 7 - Values obtained from the [1]H-NMR spectrum for the deacetylation degree calculation.

Integral of the H-C2 signal	Integral of the H-acetyl signal	Theoretical deacetylation degree (%)	Deacetylation degree obtained (%)
1.60	1.00	85.0	79.2

It can be observed that it was obtained a deacetylation degree of 79,2%, similar to the value given by the manufacturer.

ATR-FTIR analysis was carried out in order to verify if the impurities present on the original chitosan were correctly eliminated and if the characteristic bands of chitosan remained in the purified sample. The obtained spectra are shown in Fig. 20.

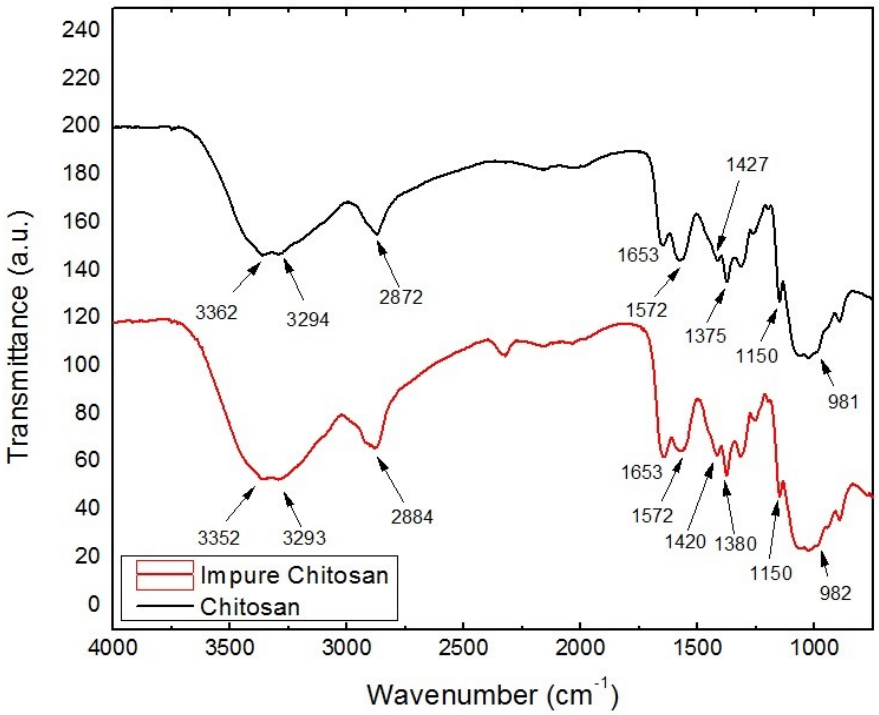

Figure 20 - Impure Chitosan (IDEBIO) and purified chitosan ATR-FTIR Spectra

The FTIR spectra of chitosan exhibited its first characteristic bands at 3362 cm^{-1} and 3294 cm^{-1} which corresponds to the – OH and – NH group stretching vibration, respectively. The stretching vibration of methylene C-H can be observed at 2872 cm^{-1}, the characteristic carbonyl C=O stretching of chitosan at 1647 cm^{-1} is attributed to the vibrations of the amide I band and the peak at 1575 cm^{-1} corresponds to the N-H deformation of amide II. The bands between 1575 cm^{-1} and 1317 cm^{-1} are characteristic of the $-CH_2$ bending vibrations and symmetric deformation vibration of $-CH_3$. The band observed at 1150 cm^{-1} corresponds to the anti-symmetric stretching of the C-O-C bridge and the band at 1063 cm^{-1} corresponds to the vibration of the pyranose structure of chitosan.

A thermogravimetric analysis was performed for both impure and purified chitosan samples to compare mass loss percentage and degradation with temperature (Fig. 21-22).

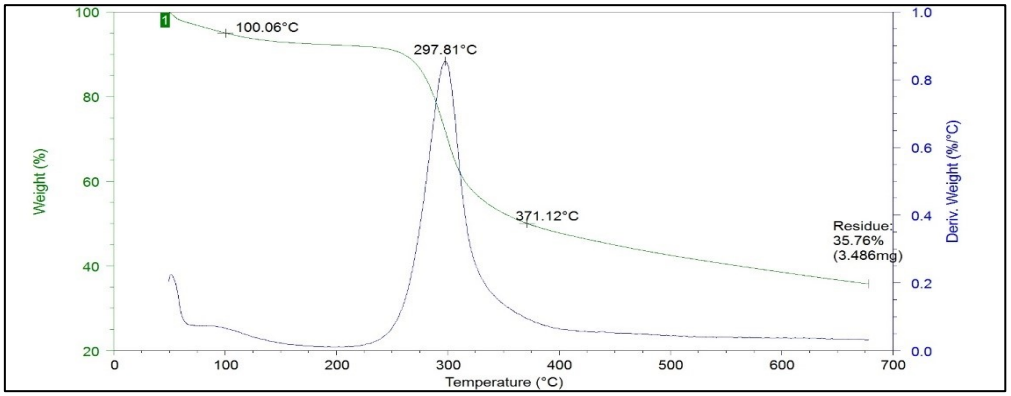

Figure 21- Impure chitosan TGA and DTGA curves

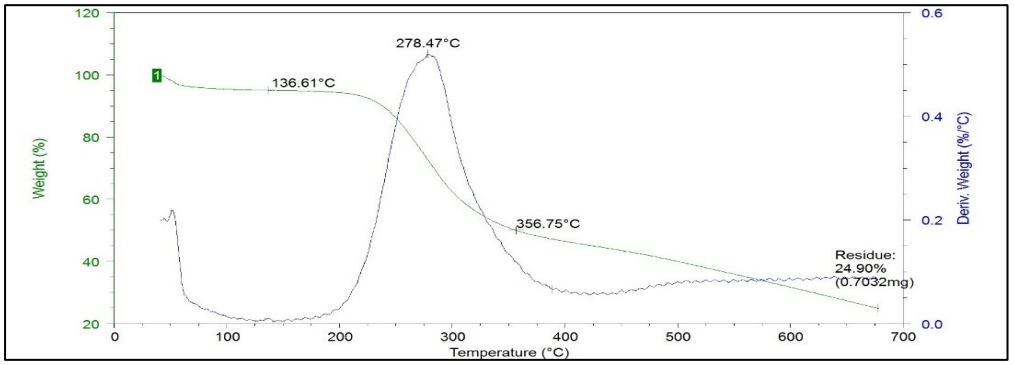

Figure 22- Purified chitosan TGA and DTGA curves

In the thermograms of both samples it's possible to distinguish three decomposition stages. The first stage occurs approximately from 50 ºC to 100 ºC and corresponds to the evaporation of the water retained in the chitosan. The second stage, which starts around 220 ºC and lasts until 400 ºC corresponds to the degradation of the saccharides of the chitosan molecular structure. The third and last stage starts around 600 ºC and corresponds to the final decomposition of the polymer. The temperatures at which both samples had 5% and 50% mass loss, the maximum temperature in the derivative curve (DTGA) and the final residue at 700 ºC were obtained and can be observed in Table 8.

Table 8- Chitosan samples values from TGA and DTGA curves.

Sample	$T_{5\%}$ (TGA) (%)	$T_{50\%}$ (TGA) (ºC)	T_{max} (DTGA) (ºC)	Residue at 700 º C (TGA) (%)
Impure Chitosan	100	371	298	36
Chitosan	137	357	278	25

As observed, the residue from the purified chitosan at 700 ºC is lower than the residue from the impure chitosan which is explained by the higher quantity of impurities in the impure sample. After analysing the results from the characterization of the purified samples, it can be confirmed that the purification process was successful.

4.3 Sodium Hyaluronate characterization

The ^{1}H-NMR spectrum obtained for HA is shown in the figure below (Fig. 23). Between 3.2 and 3.9 ppm a set of peaks corresponding to the protons of the pyranosyl ring of hyaluronate is observed. In the range 4.2-4.5 ppm two characteristic peaks of the protons of the anomeric carbons appear, which overlap with the signal of the solvent. At 1.95 ppm a characteristic peak of the three protons (-CH 3) of the N-acetyl group of the polymer is shown. This peak is often used as a reference for the calculation of modification degrees.

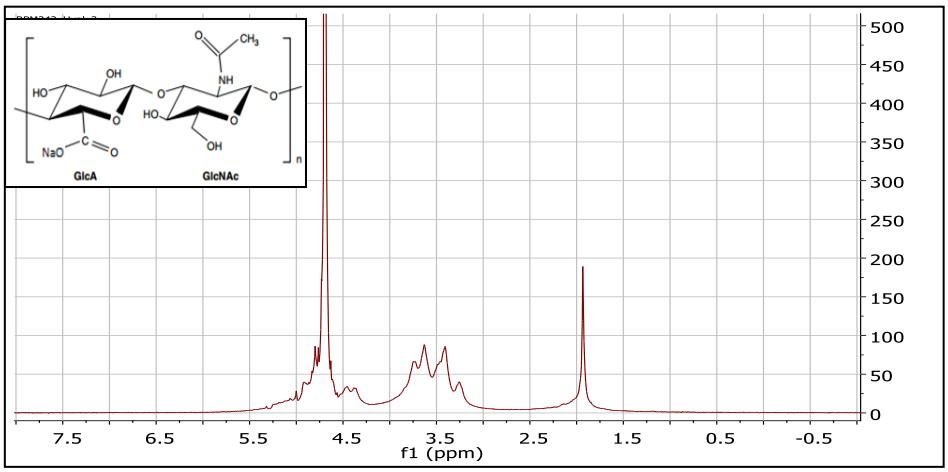

Figure 23 - 1H-NMR spectrum in D2O and scheme of the chemical structure of sodium hyaluronate of BIOIBERICA.

An ATR-FTIR analysis was also realized to better characterize the hyaluronic acid utilized (Fig. 24).

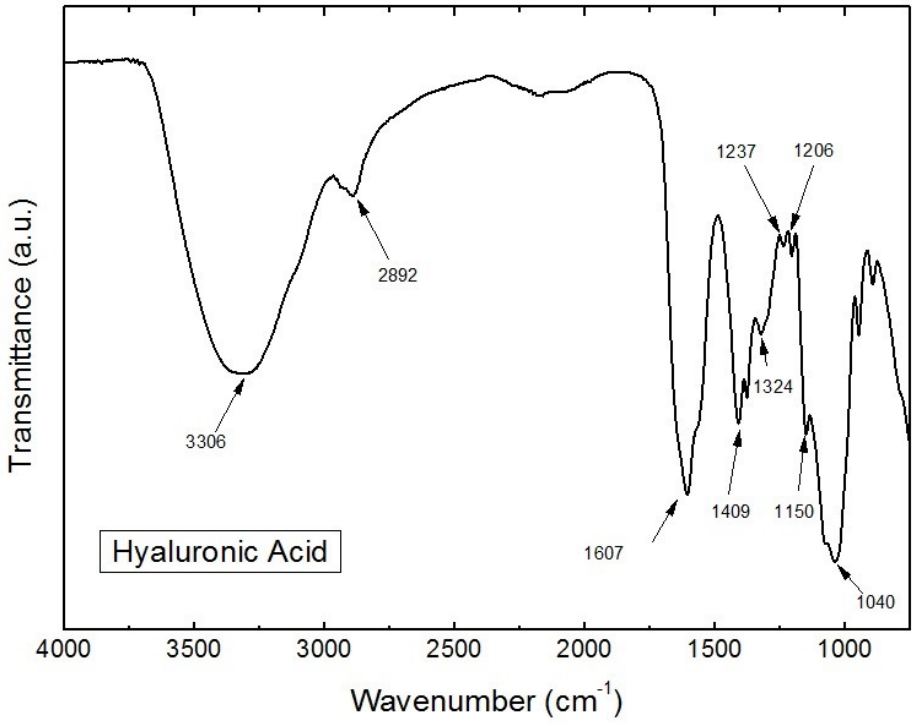

Figure 24 - Hyaluronic acid ATR-FTIR spectrum

The hyaluronic acid ATR-FTIR spectrum shows a broad band that extends from 2000 cm^{-1} to 3600 cm^{-1} which is due to the stretching bands belonging to -NH and -OH groups engaged in hydrogen bonds. The band at 2892 cm^{-1} is characteristic of -CH stretching vibrations. Between 1500 cm^{-1} and 1700 cm^{-1} appears an intense group of bands and is due to the superposition of stretching vibrations of the C=O amide (amide I) and the bending vibrations of the -NH (amide II) bands. The band at 1409 cm^{-1} could be attributed to either the symmetric carboxylate COO^- group or the stretching vibrations of the same group that exhibits asymmetry, allowing the distinction of two parts C=O and $-CO^-$ (Haxaire et al. 2003). An intense band ranging from around 950 cm^{-1} to 1200 cm^{-1} corresponds to -CO stretching vibrations, and the band appearing at 1150 cm^{-1} is due to the antisymmetric stretching vibrations of glyosidic groups.

A thermogravimetric analysis of the hyaluronic acid sample was also realized (Fig. 25) and its results are displayed in table 9.

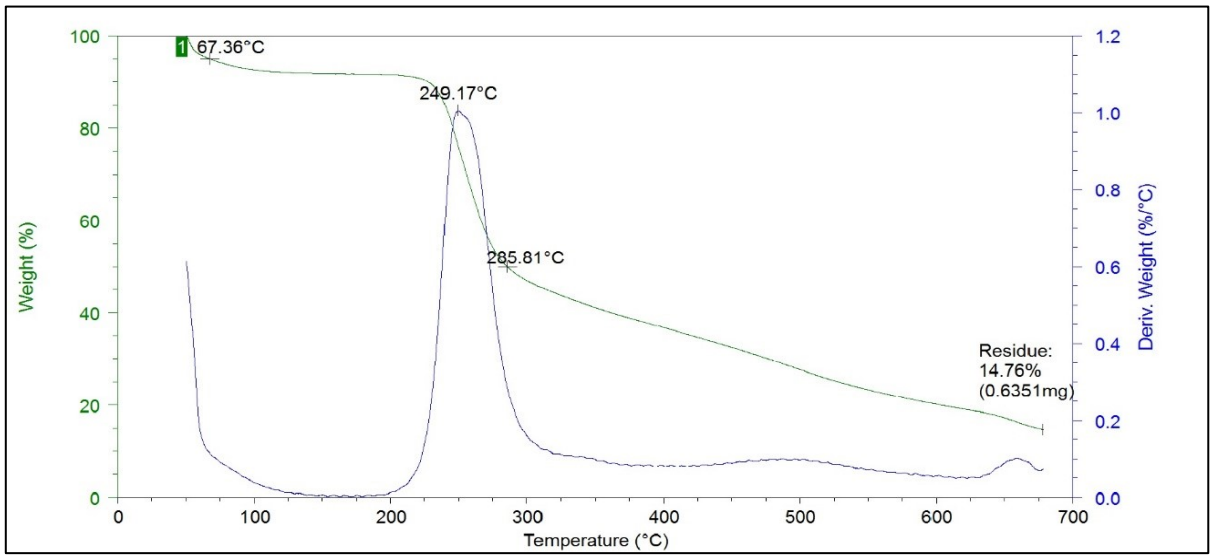

Figure 25 - Hyaluronic acid TGA and DTGA graphics

It is possible to distinguish three different decomposition stages in the TGA thermogram. The first stage occurs approximately from 50 ºC to 80 ºC and corresponds to the evaporation of the water retained in the hyaluronic acid.

The degradation of the polymer chain occurs predominantly from 200 ºC to 300 ºC, reaching the temperature peak at 249 ºC, from 300 ºC onwards the final decomposition of the polymer occurs.

Table 9- Hyaluronic acid TGA data results.

Sample	**$T_{5\%}$ (TGA) (%)**	**$T_{50\%}$ (TGA) (ºC)**	**T_{max} (DTGA) (ºC)**	**Residue at 700 º C (TGA) (%)**
Hyaluronic Acid	68	286	249	15

4.4 Preparation and characterization of Ch membranes crosslinked with GPhy

Hydrogel membranes developed in this work were based on polysaccharides, the major components being Ch and HA, and they were obtained by crosslinking of Ch with GPhy in different proportions. The most probable mechanism of the the crosslinking reaction of Ch with GPhy would be due to phosphate ions interactions with NH_3^+ cations of Ch producing the ionic crosslinking. In addition, hydrogen bonding interactions between the hydroxyl groups of the glycerol rest of GPhy and the polysaccharide may contribute to the hydrogel membrane stability.

In the first place, Ch was crosslinked with different proportions of GPhy and the resulting hydrogel membranes (Ch/GPhy) were analysed by ATR-FTIR spectroscopy. The main absorption bands in the Ch/GPhy membranes spectra and changes respect to Ch spectra are shown in Fig. 26 and they can be summarized as follows: The band between 3600 and 3000 cm^{-1} assigned to associated O-H and N-H stretching vibrations became broader and shifted to lower wavenumber (3262 cm^{-1}) whereas in the Ch spectrum this band presented peaks at 3361 and 3294 cm^{-1}. This can indicate the presence of interactions between amino groups of Ch and phosphate groups of GPhy but also between hydroxyl groups of Ch and the glycerol rest of GPhy; the band of amide I in the crosslinked Ch shifted to lower wavenumber (1633 cm^{-1}) respect to that in the plain Ch (1647 cm^{-1}); the band due to N-H deformation vibrations notably increased in the crosslinked membranes and shifted to lower wavenumber (1547 cm^{-1} versus 1575 cm^{-1} in the Ch), indicating the ionic interactions between the amino groups and phosphate groups of GPhy; the band due to C-H deformation also shifted to lower wavenumber (1407 cm^{-1} versus 1415 cm^{-1} in the Ch) and notably increased indicating the presence of more hydrocarbon bonds coming from the GPhy moieties present in the membranes; a new band in the range 1225 to 1264 cm^{-1}, depending on the GPhy concentration, appears, indicative of the presence of P=O bonds; the band centred at 1023 cm^{-1} attributed to vibration of pyranose structure and stretching of P-O and P-O-C shifted and enlarged with respect to that in Ch (1063 cm^{-1} due only to the pyranose structure) indicating the presence of C-O and C-O-P stretching vibrations due to the GPhy crosslinker; a new band at 918 cm^{-1} attributed to stretching vibratios of P-O and P-O-C in the crosslinker appears.

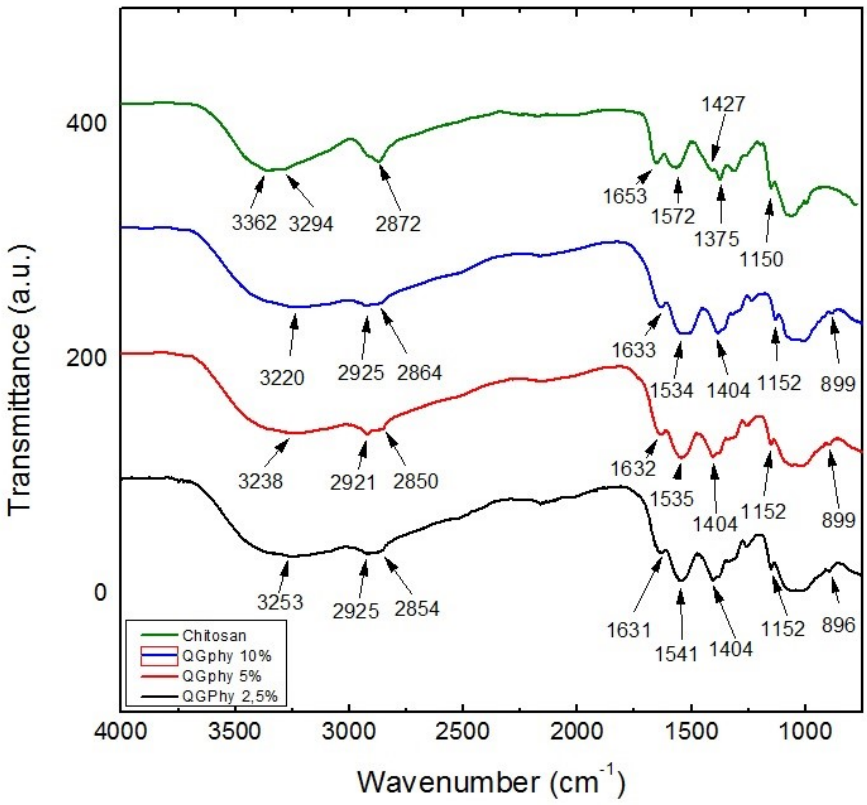

Figure 26- ATR-FTIR spectra of ChGPhy membranes at different GPhy concentrations and initial Ch.

These findings are consistent with those observed for Ch capsules crosslinked with PA (Lee et al. 2011). Their FTIR spectra revealed a shift of the band due to protonated amine group bending vibration towards 1534 cm^{-1} indicating that an ionic crosslinking has occurred at the amine group on Ch (Shu & Zhu 2002a; Shu & Zhu 2002b). In other works, the FTIR spectra of the protein nanofibrous scaffolds crosslinked with PA (Ravichandran et al. 2013) showed also differences compared to the pure (non-crosslinked) material (Ishiguro et al. 2003).

Elemental analysis of crosslinked Ch membranes was performed to determine the analysis of C, H and N. Results are given in Table 10. A clear increase in the C/N relationship of the membranes was observed with respect to Ch due to the presence of GPhy.

Table 10- Elemental analysis results of initial Ch and GPhy crosslinked Ch membranes.

Sample	% C	% H	% N	C/N
Ch	38.90	6.93	7.23	5.38
ChGphy2.5	36.08	7.06	5.64	6.39
ChGphy5	36.67	7.00	5.64	6.50
ChGphy10	35.80	6.89	5.53	6.47

Scanning electron microscopy (SEM) and energy dispersive X-ray spectroscopy (EDX) analysis were applied to assess the surface morphology of the xerogel membranes and their elemental composition. Results are shown in Fig. 27-29. Surface morphology of the membranes was predominantly smooth independent of the content of GPhy.

The EDX spectra of Ch membranes showed the peaks of the main elements C, O, N at the characteristic energy levels of 0.27, 0.52, 0.39 keV respectively. In addition, a peak at the energy level of phosphorous (2.01 keV) belonging to the GPhy polyanions was observed confirming the crosslinking reaction. The C/O ratios of the membranes slightly decreased giving values of 0.95, 0.93 and 0.89 with increasing concentration of GPhy indicating the presence of a higher concentration of O coming from the GPhy. Meanwhile, the C/P ratios notably decreased with the content of GPhy giving values of 89.72, 52.75 and 34.00. Similar results were reported for electrospun protein nanofibers crosslinked with PA (Ravichandran et al. 2013).

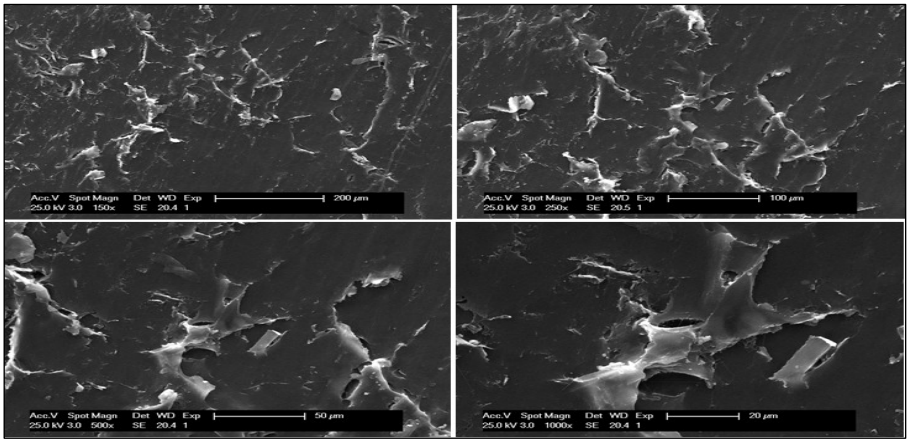

Figure 27 - Figure 30 - SEM Images of ChGPhy 2,5% membrane (200 µm upper-left, 100 µm upper-right, 50 µm lower-left, 20 µm lower-right).

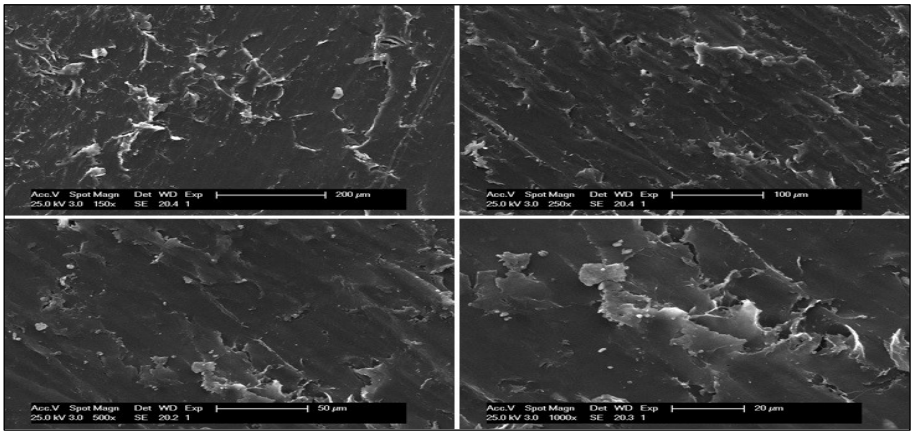

Figure 28 - SEM Images of ChGPhy 5% membrane (200 µm upper-left, 100 µm upper-right, 50 µm lower-left, 20 µm lower-right).

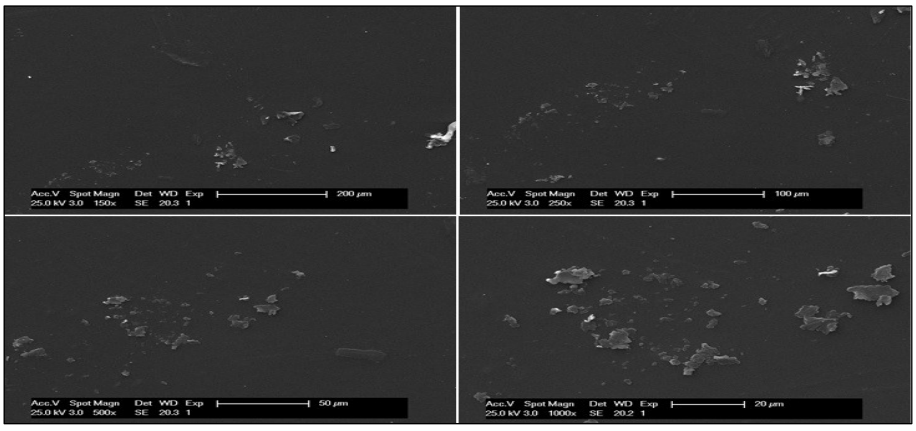

Figure 29 - SEM Images of ChGPhy 10% membrane (200 µm upper-left, 100 µm upper-right, 50 µm lower-left, 20 µm lower-right).

Thermal degradation of ChGPhy membranes was analysed by thermogravimetry. TGA and DTGA curves are shown in Fig. 30-32 and the values obtained summarized in table 11. All the thermograms exhibited two steps. The first one occurred bellow 130ºC, which is associated with the loss of water by evaporation. The second and main degradation step with maximum decomposition rate around 278ºC has been associated with the dehydration of the saccharide rings, depolymerization and decomposition of molecular units of the Ch chain (Fernández-quiroz et al. 2015). It is worth noting that for the ChGPhy10 sample a broad maximum in its DTGA appeared at 450ºC coinciding with the last stage of decomposition of GPhy. All membrane samples had values of residues higher than plain Ch showing again the presence of phosphates in the samples.

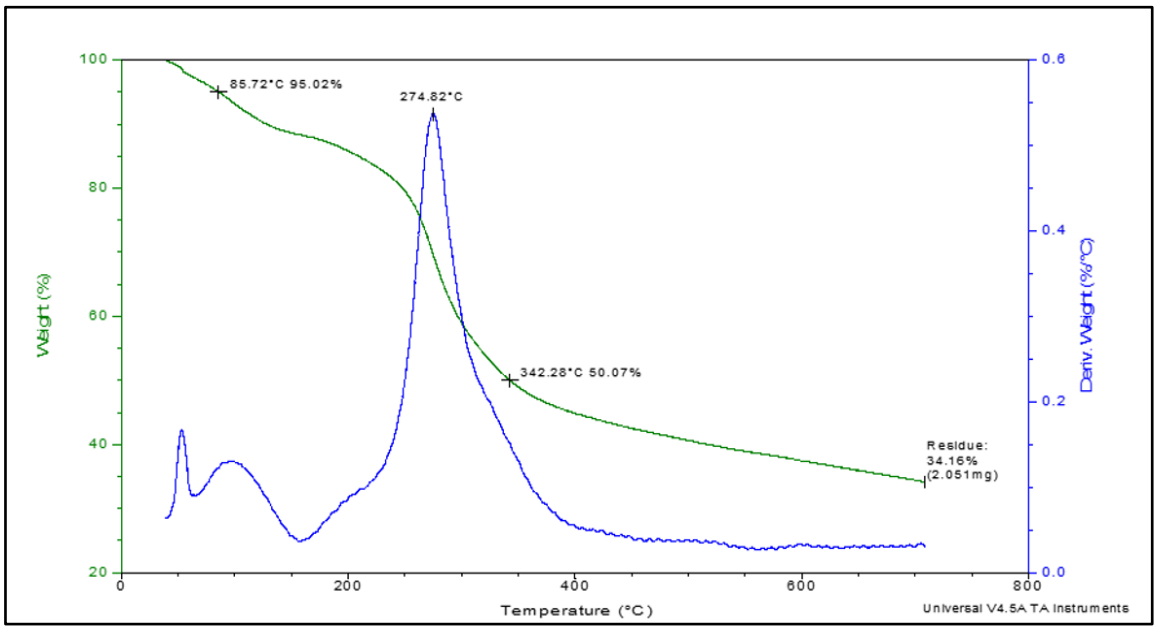

Figure 30 - ChGPhy2.5 TGA and DTGA curves.

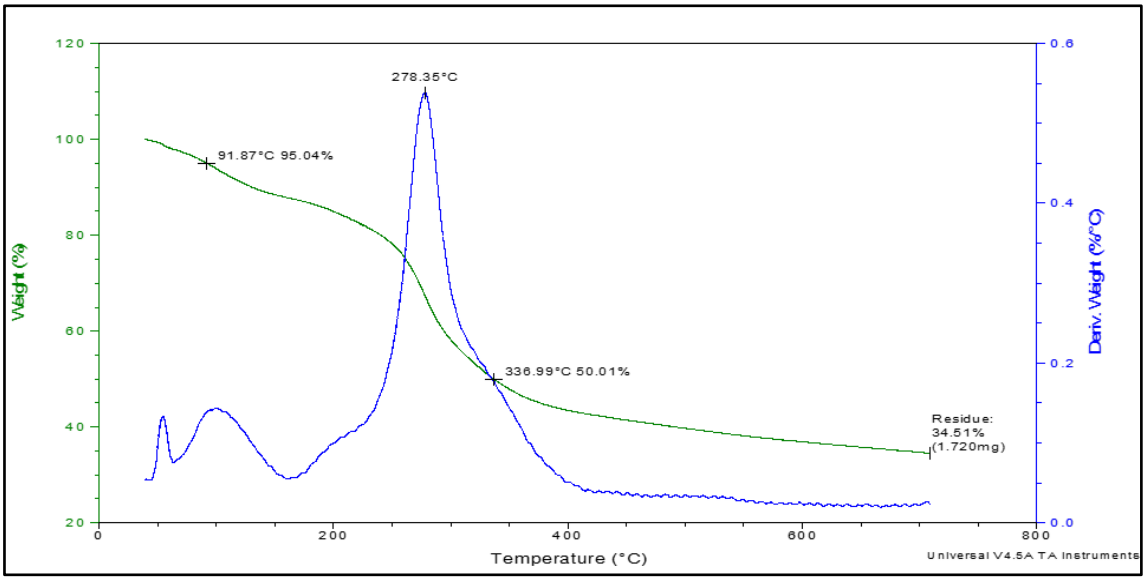

Figure 31 - ChGPhy5 TGA and DTGA graphic.

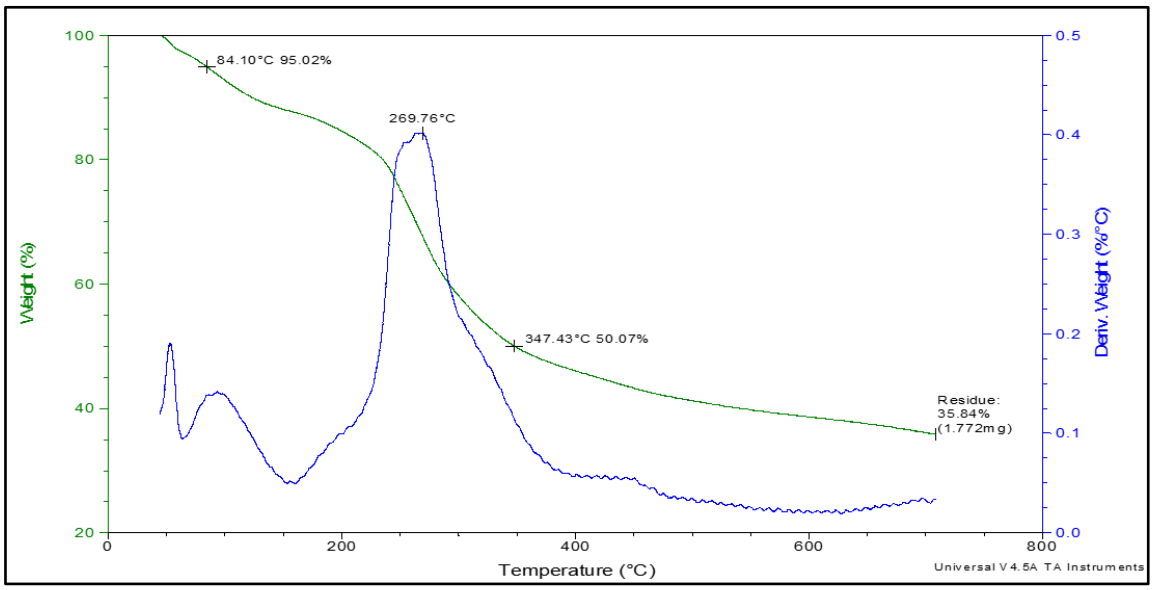

Figure 32- ChGPhy10 TGA and DTGA graphic.

Table 11 - Thermal degradation results of Ch membranes crosslinked with GPhy.

Sample	T_{max} main step (ºC)	Residue (%)
Ch	278	25
ChGPhy2.5	275	34
ChGPhy5	278	35
ChGPhy10	263	36

4.5 Preparation and characterization of Ch/HA membranes crosslinked with GPhy

GPhy crosslinked membranes containing more than one polysaccharide were fabricated with mixtures of Ch and HA in a Ch:HA ratio of 60:40. The crosslinking reaction was carried out in a slightly acidic medium in order to guarantee solution of both polysaccharides. Under these conditions the crosslinking reaction will be due to the ionic interactions between the phosphate anions of GPhy and the protonated amino groups of Ch. The resulting material will be a semi-interpenetrated network (semi-IPN) formed by crosslinked Ch and linear HA. However, most probably, intermolecular interactions such as hydrogen bonding can occur intervening the carboxylic and hydroxyl groups of HA and hydroxyl and amino groups of Ch giving a dimensional stability to the resulting semi-IPN hydrogel structure. The ATR-FTIR spectra of Ch/HA membranes are shown in Fig. 33.

The spectra showed the characteristic bands of both polysaccharides along with those of GPhy crosslinker. Moreover, the wavenumber of the bands belonging to Ch coincides with that found in Ch/GPhy samples. The main bands appeared at 3266 cm^{-1} (υ O-H and N-H associated), 2924 and 2854 cm^{-1} (υ C-H), 1736 cm^{-1} (υ C=O in carboxylic groups), 1631 cm^{-1} (υ C=O in amide, amide I), 1521 cm^{-1} (δ N-H), 1415 cm^{-1} (υ COO- and δ C-H), 1376 cm^{-1} (δ - CH_3 symmetrical), 1236 cm^{-1} (υ P=O), 1151 cm^{-1} (υ C-O-C asymmetric), 1021 cm^{-1} (vibration of pyranose structure and υ P-O and P-O-C) and 900 cm^{-1} (υ P-O and P-O-C).

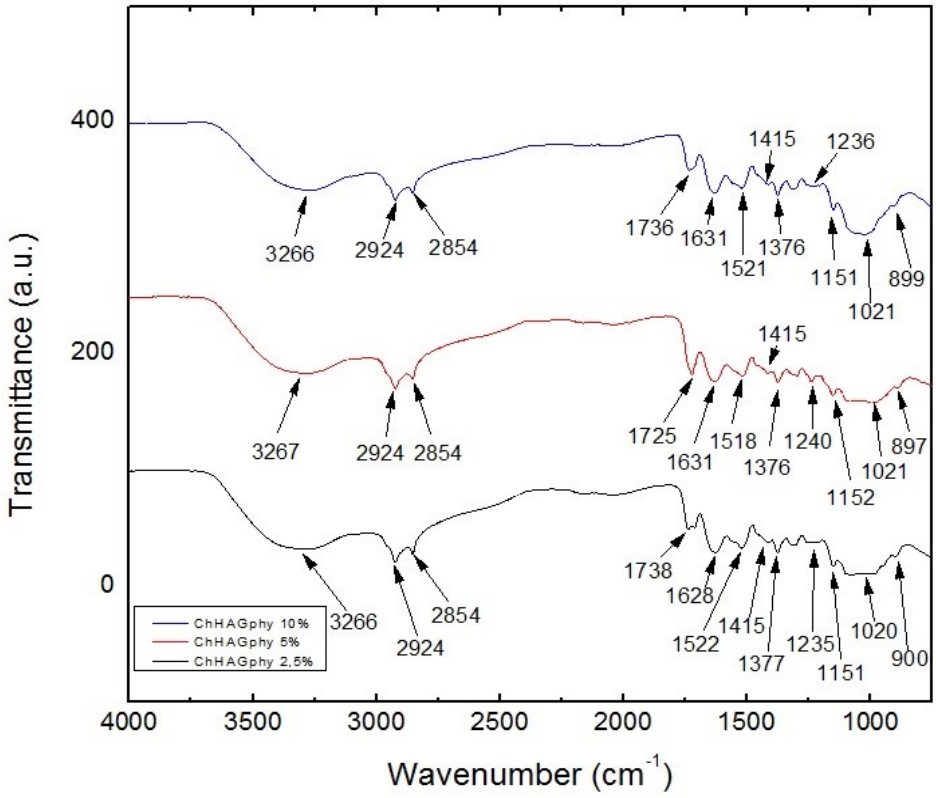

Figure 33 - ATR-FTIR of 1-6:4ChHA membranes at different GPhy concentrations.

The content of free amino groups in the hydrogels after the reaction of Ch with GPhy in presence of HA was determined by pH titration. The results are shown in Fig. 34. Analysis of the curves provided a content of free amino groups of 45 % for membranes crosslinked with 2.5% GPhy and of 42 and 43% for those crosslinked with 5 and 10% GPhy respectively. Considering that the deacetylation degree of the plain Ch was 85%, these results indicate a notable reduction of free amino groups after the ionic crosslinking in all cases.

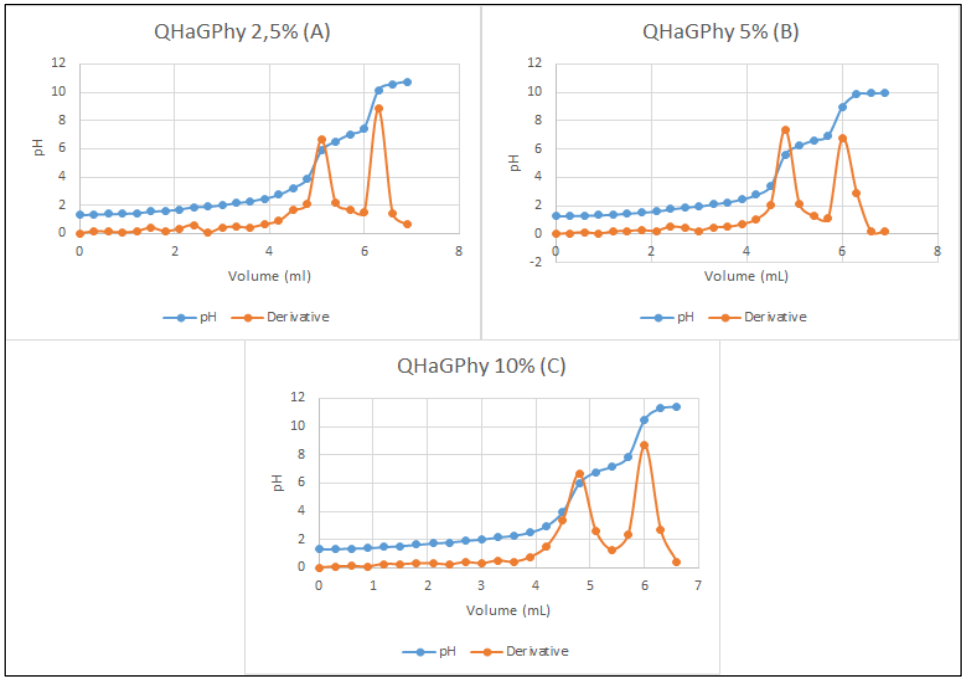

Figure 34 – Free amino group graphics for (A) 6:4ChHA2.5, (B) 6:4ChHA5 and (C) 6:4ChHA10 membranes.

The Ch/HA membranes were characterized by elemental analysis and results are displayed in Table 12. The C/N ratio of membranes oscillated between those of initial polysaccharides showing a slight tendency to increase with the content of GPhy. The C/N ratio of these membranes was somewhat higher than that of Ch/GPhy membranes due to the higher value of this ratio in the HA.

Table 12 - Elemental analysis results of initial Ch and GPhy crosslinked Ch membranes.

Sample	% C	% H	% N	C/N
Ch	38.90	6.93	7.23	5.38
HA	33.01	5.92	2.93	11.27
6:4ChHA2.5	32.83	6.04	5.04	6.54
6:4ChHA5	31.52	6.16	4.69	6.72
6:4ChHA10	31.21	6.03	4.73	6.59

Surface morphology of Ch:HA membranes was examined by SEM studying the influence of Ch:HA. Fig. 35 and Fig. 36 shows the SEM images of Ch:HA membranes with a Ch:HA ratio of 50:50 and 60:40, respectively. A highly porous well-structured morphology was observed in all samples independent on Ch:HA ratio. This surface morphology seems to be very adequate for the colonization and proliferation of cells in tissue engineering applications.

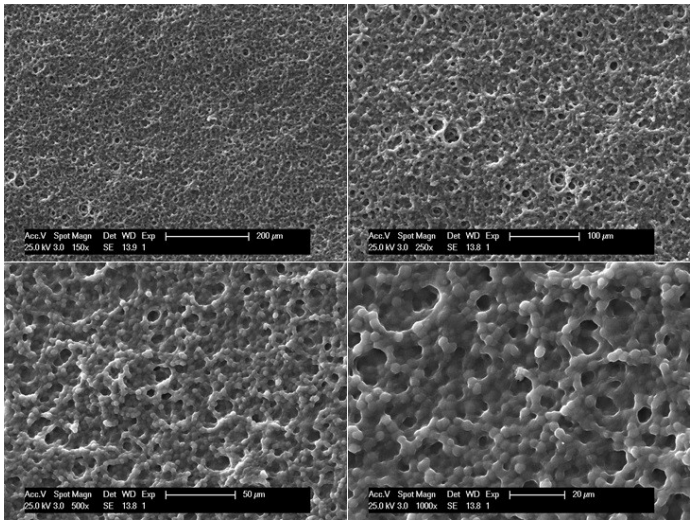

Figure 35 - SEM Images of 5:5 Ch/HA 5% membrane (200 µm upper-left, 100 µm upper-right, 50 µm lower-left, 20 µm lower-right)

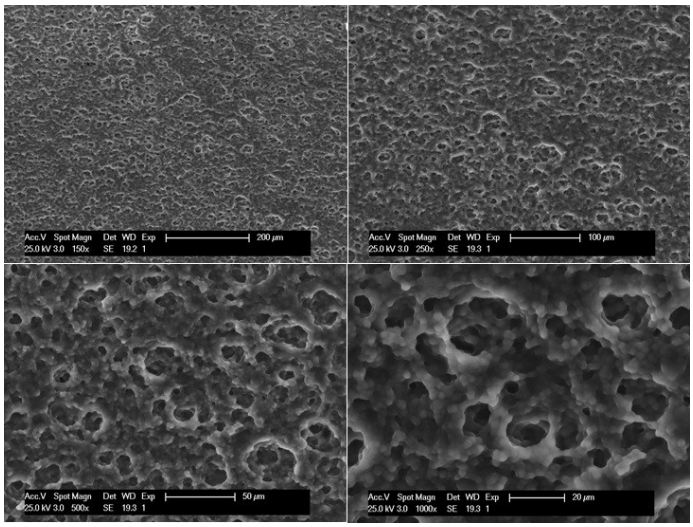

Figure 36 - SEM Images of 6:4 Ch/HA 5% membrane (200 µm upper-left, 100 µm upper-right, 50 µm lower-left, 20 µm lower-right)

Thermal degradation of Ch/HA membranes was analysed by thermogravimetry. TGA and DTGA curves are shown in Fig. 37-39 and the results obtained are summarized in table 13. The degradation pattern of all membranes was independent of GPhy concentration, showing a main degradation step with maximum rate around 200ºC in which the depolymerisation and decomposition of molecular units of both polysaccharide chain take place. A peak around 150ºC was observed in the DTGA curves which can be associated to the loss of water. In addition, a shoulder at around 275ºC was observed in all membranes also associated to degradation of both polysaccharides. It must be mentioned that thermal stability of the Ch/HA semi-IPNs was lower than that of Ch membranes due to the lower thermal stability of initial HA.

Regarding residue, in all semi-IPNs samples it increased with respect to plain Ch and HA.

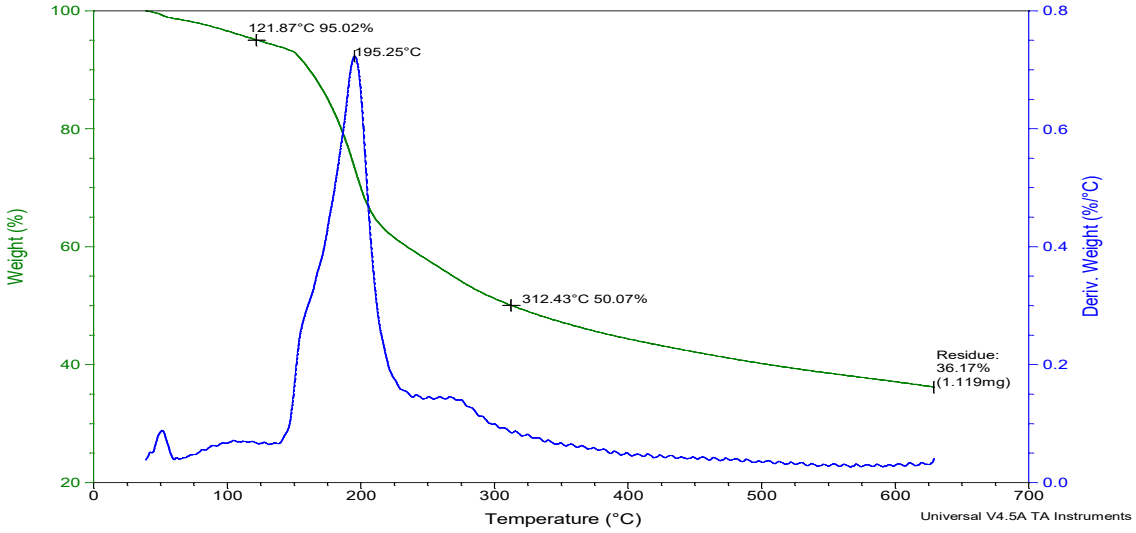

Figure 37 - 60:40ChHA2.5 TGA and DTGA graphics.

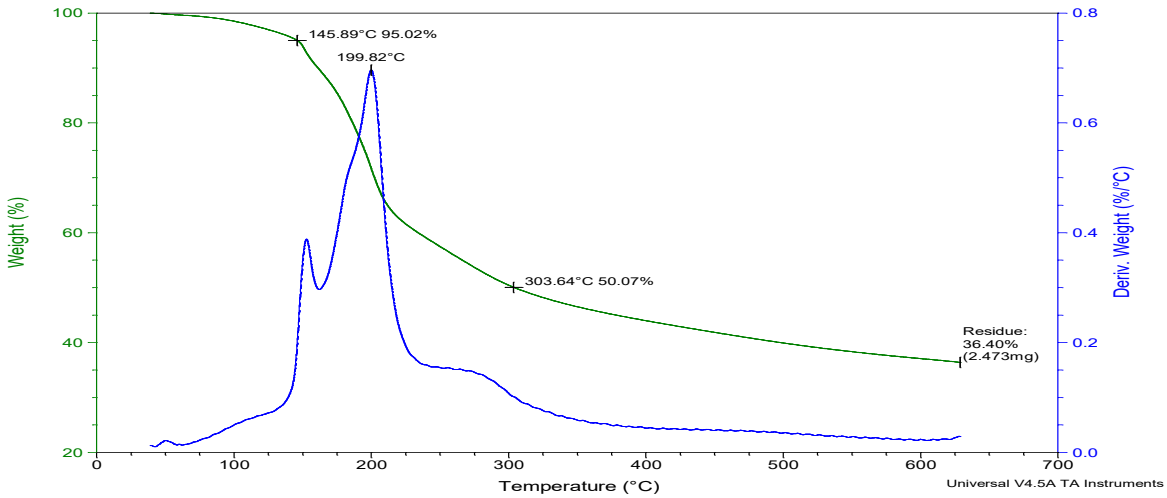

Figure 38 - 60:40ChHA5 TGA and DTGA graphics.

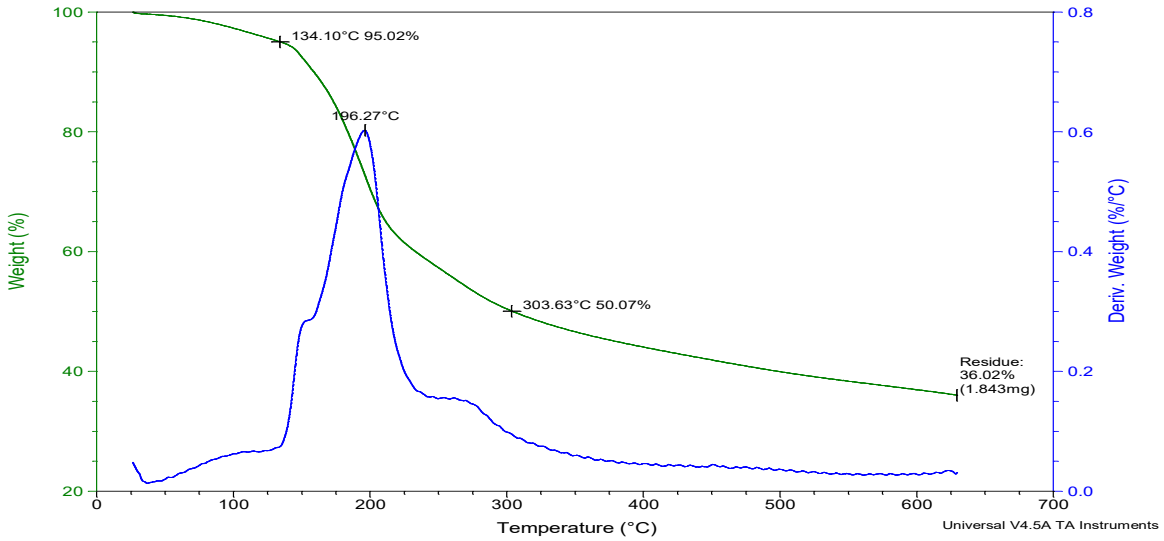

Figure 39 - 60:40ChHA10 TGA and DTGA graphics.

Table 13 - Thermal degradation results of ChHA membranes crosslinked with GPhy.

Sample	T_{max} main step (ºC)	Residue (%)
Ch	278	25
HA	249	15
6:4ChHA2.5	195	36
6:4ChHA5	200	36
6:4ChHA10	196	36

Part II

Due to the favorable results obtained in Part I it was decided to use a medical grade chitosan and change the synthesis process of GPhy in order to avoid using acidic pH during its synthesis. The new GPhy synthesis was done according to subchapter 3.2.2. All results presented in this subchapter were obtained using chitosan from Altkatin and the new GPhy.

4.6 Synthesis and characterization of the GPhy crosslinker

In this example, GPhy crosslinking agent was synthesized by a condensation reaction between PA and G in a PA:G molar ratio of 1:7, the crosslinker was named GPhy1:7. The purified crosslinker was characterized by ATR-FTIR spectroscopy along with its precursors, G and PA. The ATR-FTIR spectra of the crosslinker showed the main representative bands present in the spectra of both precursors. Particularly for GPhy1:7, a broad band at 3248 cm^{-1} due to stretching vibrations of O-H and N-H associated bonds; bands at 2943 and 2888 cm^{-1} due to asymmetric and symmetric vibrations of C-H bonds of the inositol ring.

At lower wavenumber, a band at 1460 cm^{-1} due to δ C-H bonds of the inositol ring and G residues, band that notably increased and it was shifted respect to PA (1399 cm^{-1}); a band at 1176 cm^{-1} attributed to υ P=O, also shifted respect to PA (1186 cm^{-1}); an intense peak at 1035 cm^{-1} (shoulder at 1004 cm^{-1}) attributed to υ C-O alcohols, υ P-O and P-O-C, and υ C-O glycosidic linkages; finally, peaks at 918, 815 (weak) and 715 (weak) cm^{-1} due to υ P-O and P-O-C bonds (Govindaraju et al. 2000), also changed respect to PA.

The crosslinker was subsequently characterized by NMR spectroscopy. Figure 40 shows ^{1}H NMR spectra of the crossliker and its precursors. Spectrum of glycerol showed a multiplet between 3.5 and 3.8 ppm that can be assigned to $^{1}CH_2$-, $^{2}CH_2$- and CH proton (Ishiguro et al. 2003). Spectrum of GPhy1:7 showed modified signals in the range of those of initial glycerol and new signals in the range 3.82 – 3.98 ppm, attributed to CH_2-O-P, and in the range 3.98 – 4.10 ppm, due to CH-O-P in the reacted glycerol moieties, respectively.

Finally, between 4.1 and 4.6 ppm, three signals of very low intensity for the GPhy1:7 crosslinker, assigned to protons H_1-H_5 protons in unmodified PA. Resonance of proton H_6 in the PA residue was not appreciated (Crimella et al. 1992).

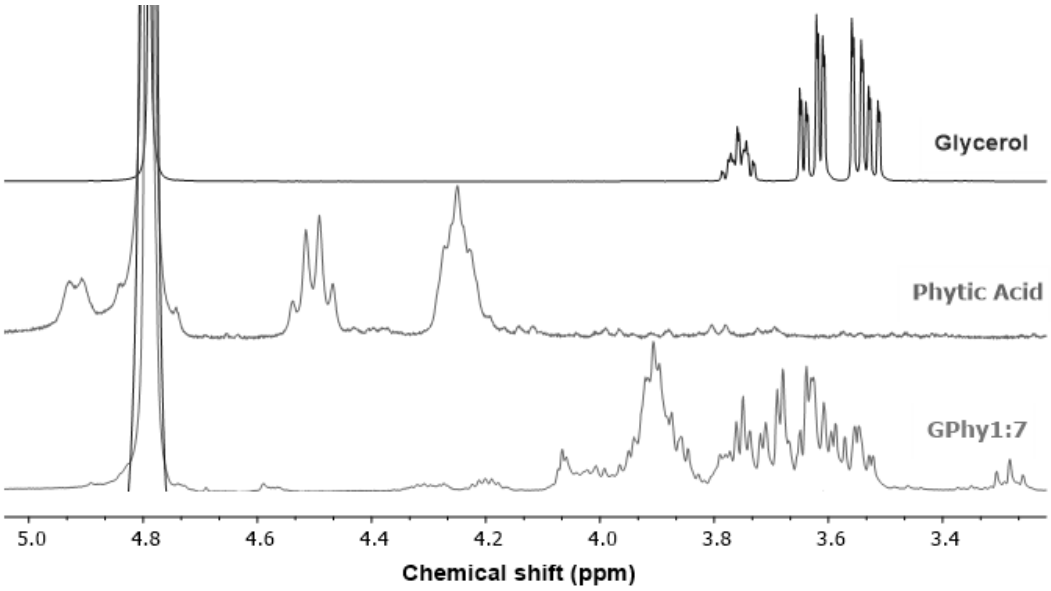

Figure 40 - ^1H NMR spectra of PA, G and GPhy1:7 in D2O at 25ºC.

The ^{31}P NMR spectrum of PA is widely discussed in literature and the majority of authors reported the resonance of four peaks (Martin et al. 1987; O'Neill et al. 1980; Turner et al. 2003). The ^{31}P NMR spectrum of the commercial PA analysed in this work (Fig. 41) showed peaks in the range -2 to 2 ppm which were assigned to P_5 (δ 0.4), P_1 and P_3 (δ 0.04), P_4 and P_6 (δ 0.53) and P_2 (δ 0.94) according to Turner el al (Turner et al. 2003). The ^{31}P NMR spectrum of GPhy1:7 (Fig. 38) showed peaks in the range -3 to 3 ppm, indicating that the chemical environment of the P nuclei changed after condensation reaction.

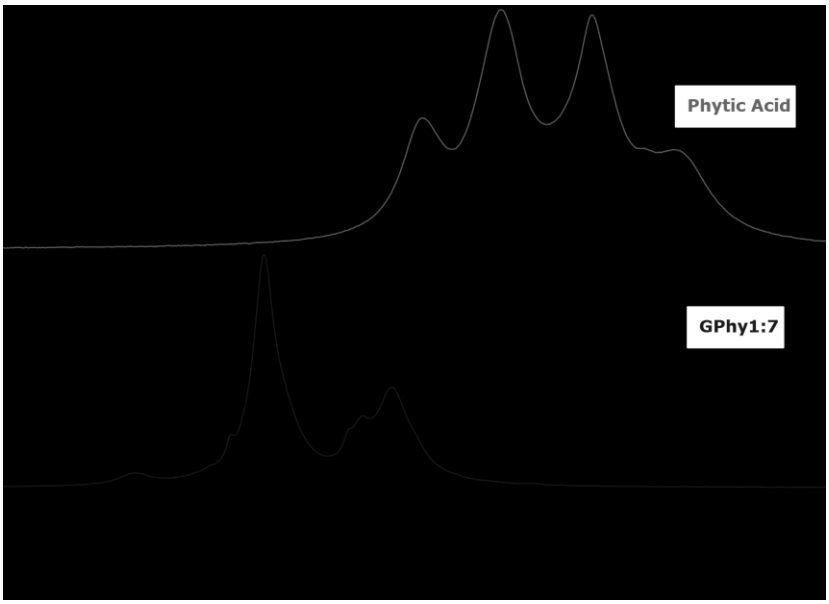

Figure 41- ^{31}P NMR spectra of initial PA and GPhy1:7 in D_2O at 25 ºC.

Thermal properties of GPhy crosslinkers were analysed by DSC and TGA techniques. DSC thermogram of GPhy1:7 showed a glass transition with a glass transition temperature (T_g) of 47ºC indicating an amorphous character of this crosslinker as a consequence of the presence of glycerol moieties in its structure. However, GPhy4:1, GPhy5:1 and GPhy6:1 did not show glass transitions what was attributed to higher contents of PA in these crosslinkers. Thermogravimetric (TGA) and differential thermogravimetric (DTGA) data of the GPhy crosslinker and precursors are shown in table 14. Weight loss of GPhy1:7 underwent in three steps. The first one with a T_{max} around 125ºC can be attributed to the loss of water contained in the sample. Second degradation step with maximum rate at 215ºC would involve the degradation of the G rest (T_{max}=228ºC) and part of the phytate residues (T_{max}=215ºC) and the last step with maximum rate at 337ºC would correspond to degradation of the phytate moiety. The residue of GPhy1:7 was 52%. This value was notably reduced with respect to that of PA, indicating the content of G, which gives no residue at all. From residue values of both GPh1:7 and PA, it was estimated the amount of G incorporated in this crosslinker after condensation reaction, which was 3 mole %.

Table 14 - Thermal degradation results of GPhy1:7 and precursors under nitrogen atmosphere.

Sample	T_{max} (ºC)				Residue (%)
	1st stage	2nd stage	3rd stage	4th stage	
G	228				0
PA	117	215	332	394	75
GPhy1:7	125	215	337	-	52

Cytotoxicity of the GPhy crosslinker was analysed using human fibroblasts (Fig. 42). The cell viability was around 70% in a concentration range of 5 - 80 mg/mL, indicating absence of cytotoxicity according to the assessment of the standard ISO 10993-5:2009 (ISO/EN10993-5,2009). From the linear portions of the corresponding curves the IC_{50} was determined as the concentration that depressed MTT-formazan production by 50%. For comparison purposes the cytotoxicity of PA and commercial β-GP were analyzed under the same experimental conditions and IC_{50} values were 8 and 9 mg/mL, respectively. Our results demonstrated that biocompatibility of the GPhy crosslinker increased respect to phytate crosslinkers currently used in literature.

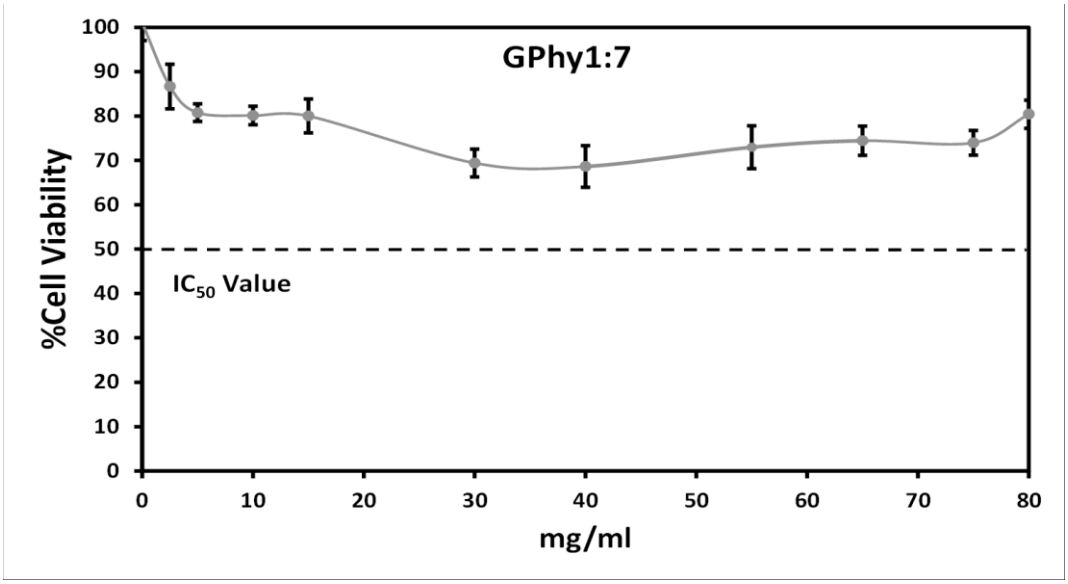

Figure 42 - Cell viability of human fibroblasts response to different concentrations of GPhy1:7.

4.7 Preparation and characterization of chitosan membranes crosslinked with GPhy1:7

Membranes were obtained by crosslinking Ch with GPhy1:7 in different proportions (hereinafter, ChGPhy1:7 membranes). The names and composition of Ch membranes prepared with this GPhy crosslinker are reported in Table 15. The most probable mechanism of the crosslinking reaction would be due to ionic interactions between phosphate anions of the crosslinker and NH_3^+ groups of Ch. In addition, hydrogen bonding interactions between GPhy1:7 crosslinker and polysaccharide may contribute to the membrane stability.

Table 15 - Names and composition of ChGPhy1:7 membranes.

Sample name	GPhy1:7 (wt-% respect to Ch)
Ch2.5%(1:7)	2.5
Ch5%(1:7)	5
Ch10%(1:7)	10

ChGPhy1:7 membranes were analysed by ATR-FTIR spectroscopy. The main absorption bands in the ChGPhy1:7 membranes spectra and changes respect to Ch spectrum are shown in Fig. 43 and they can be summarized as follows: the band between 3600 and 3000 cm^{-1} assigned to associated υ O-H and N-H became broader, what can indicate the presence of interactions between amino groups of Ch and phosphate groups of GPhy1:7 but also between hydroxyl groups of Ch and G molecules of GPh1:7; a new peak appears at 2972 cm^{-1} and increases with the GPhy1:7 crosslinker content; bands in the range 1700 -1500 cm^{-1} became broader, the band at 1647 cm^{-1} due to amide I reduced, the band at 1582 cm^{-1} due to δ N-H shifted to lower wavenumber respect to Ch (1588 cm^{-1}) indicating ionic interactions between the amino groups and phosphate groups of GPhy and a shoulder at 1540 cm^{-1} appears and increases with the crosslinker content; in the range 1100 y 1000 cm^{-1} the peak at 1066 cm^{-1} increases and the peak at 992 cm^{-1} decreases and shifted to 998 cm^{-1} with the content of GPhy1:7 in the membrane.

Our FTIR results are consistent with those reported for Ch (Shu & Zhu 2002a; Shu & Zhu 2002b) and proteins (Ravichandran et al. 2013; Cui et al. 2010) crosslinked with PA.

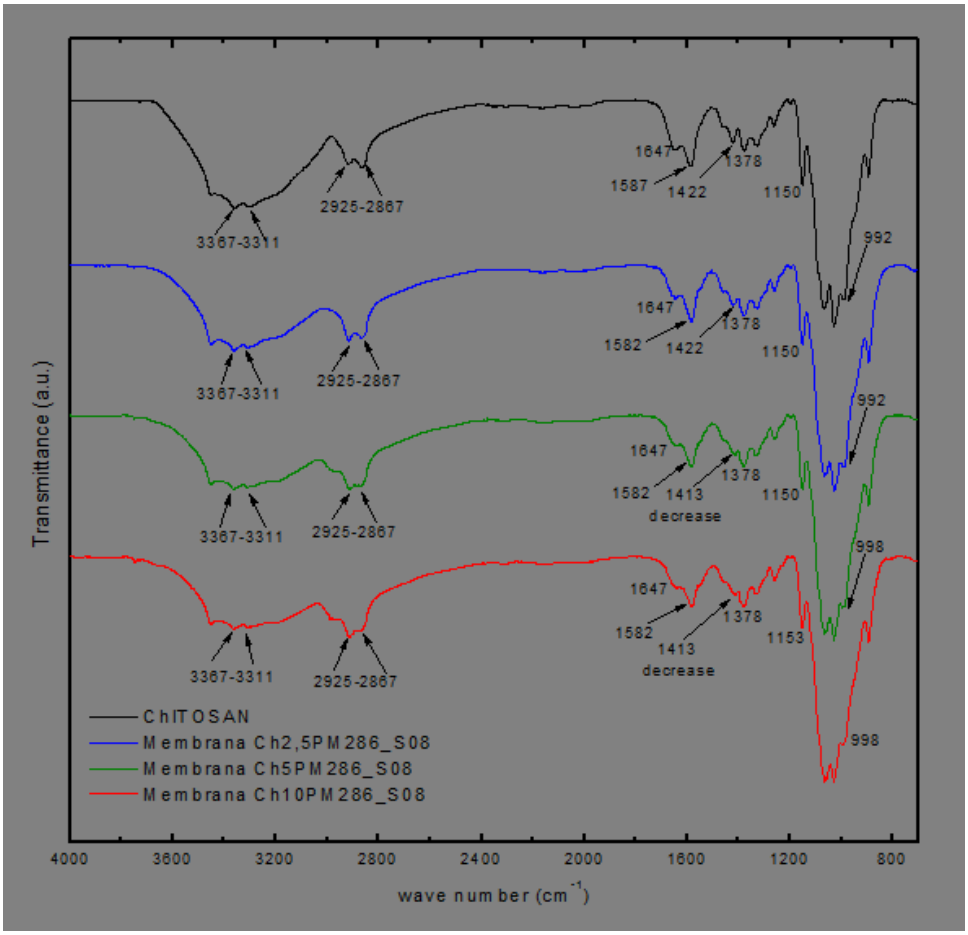

Figure 43 - ATR-FTIR spectra of ChGPhy1:7 membranes and initial Ch.

SEM and EDX analysis were applied to assess the surface morphology and elemental composition of membranes. Surface morphology of the membranes was predominantly smooth independent of the content of GPhy1:7. The EDX spectra of ChGPhy1:7 membranes showed the peaks of the main elements C, O, N at the characteristic energy levels of 0.27, 0.52, 0.39 keV respectively. In addition, a peak at the energy level of P (2.01 keV) belonging to the GPhy1:7 polyanions was observed, confirming the crosslinking reaction. EDX data of membranes are given in Table 16.

Table 16 - EDX results of ChGPhy1:7 membranes.

Membrane	C/N	C/O	C/P	N/P
Ch2.5%(1:7)	4.6	1.1	361.5	78.5
Ch5%(1:7)	4.2	1.1	126.7	30.0
Ch10%(1:7)	4.0	3.5	104.8	25.8

The C/O ratio slightly increased with concentration of crosslinker indicating the presence of a higher content of O coming from the GPhy1:7, whereas the C/P and N/P ratios notably decreased. Similar results were reported for electrospun protein nanofibers crosslinked with PA (Ravichandran et al. 2013).

Thermal degradation of ChGPhy1:7 membranes was analysed by TGA under air atmosphere and results are shown in Table 17. Degradation of membranes occurred in two main steps, the first one with maximum rate at around 300ºC and the second one *circa* 600ºC. Thermal degradation of ChGPhy1:7 membranes can be mainly associated with the dehydration of the saccharide rings, depolymerization and decomposition of molecular units in the Ch chains (Fernández-quiroz et al. 2015). All ChGPhy1:7 membranes samples presented residues showing the presence of phosphates in the samples coming from the GPhy1:7 crosslinker.

.

Table 17 - TGA and DTGA results of ChGPhy1:7 membranes under air atmosphere

Sample	T_{max}		Residue (%)
	1st stage	2nd stage	
Ch	306	582	0
Ch2.5%(1:7)	296	599	2.0
Ch5%(1:7)	290	598	1.4
Ch10%(1:7)	287	582	1.55

Swelling behaviour of crosslinked membranes was studied in PBS of pH 7.4 at 37ºC. Evolution of swelling with time is displayed in Fig. 44. Water uptake was very fast reaching a maximum at 1 day for all samples. At this time, the membrane crosslinked with 5% GPhy1:7 reached a value *circa* 100% whereas the membranes crosslinked with 2.5 and 10% GPhy1:7 around 85%, indicating that 5% can be an optimum crosslinker concentration. At 2 days, water uptake slightly decreased although not significantly. This result is usually associated with the elastic behaviour of polymers in which relaxation of the macromolecules is produced as a consequence of the immersion in a hydration medium. At 7 days, water uptake stabilized for Ch5%(1:7) and Ch10%(1:7) membranes, whereas it significantly decreased for those fabricated with 2.5% of crosslinker.

This swelling decrease can be due to breaking of some ionic crosslinks what is more evident in the less crosslinked samples. The swelling of uncrosslinked Ch samples also significantly decreased which can be attributed to disintegration in the medium. Then, 2.5% GPhy1:7 concentration seems not to be enough to give membrane stability in the short time. On the contrary, we can say that both 5 and 10% of GPhy1:7 concentrations provided membranes with adequate swelling behaviour and stability to be used in biomedical applications.

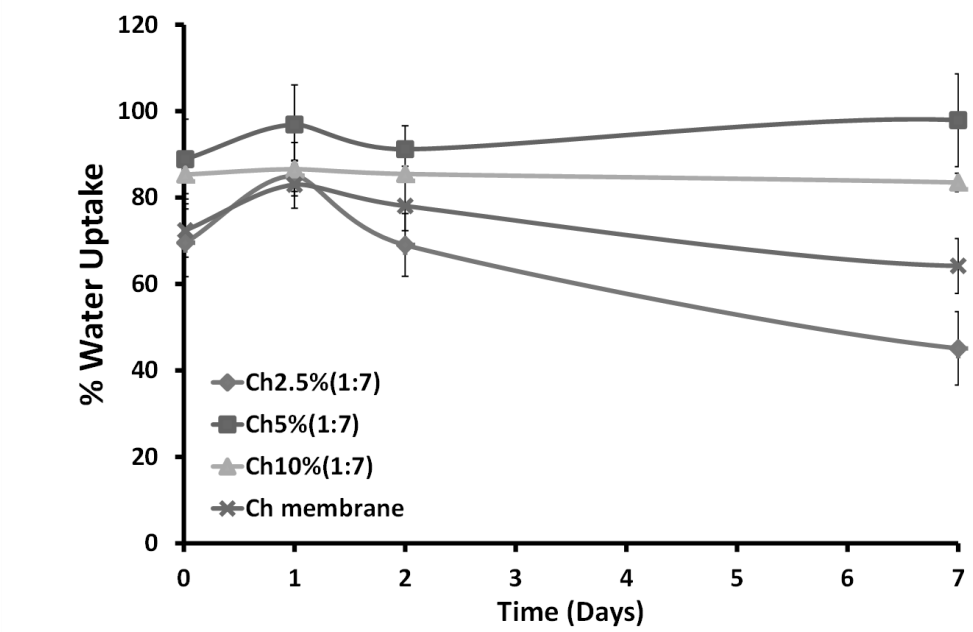

*Figure 44 - Water uptake of ChGPhy1:7 membranes in PBS (pH 7.4, 37ºC). Results are given as mean ± sd (n=5). Statistical analysis (ANOVA) of each sample was performed at times 2 and 7 days with respect to 1 day (*p<0.05).*

4.8 Preparation and characterization of Ch/HA membranes crosslinked with GPhy1:7

Crosslinked membranes containing more than one polysaccharide were fabricated with mixtures of Ch and HA in a Ch:HA mass ratio of 60:40 using GPhy1:7 as a crosslinker (hereinafter, Ch/HAGPhy1:7 membranes). As for ChGPhy1:7 membranes, the crosslinking reaction will be due to ionic interactions between the phosphate anions of GPhy1:7 and the protonated amino groups of Ch. However, in this case, the resulting material will be a semi-interpenetrated polymer network (semi-IPN) formed by a network of crosslinked Ch in which linear HA macromolecules are entangled with those of Ch. In addition, intermolecular interactions such as hydrogen bonding, intervening the carboxylic, hydroxyl groups and amino groups belonging to different polysaccharides can most probably occur, contributing to the dimensional stability of the semi-IPN hydrogel structure. Names and composition of the as produced membranes is given in Table 18.

Table 18 - Names and composition of the Ch/HAGPhy1:7 membranes.

Sample name	Ch/HA (wt/wt)	GPhy1:7 (wt % respect to Ch)
Ch/HA2.5%(1:7)	60:40	2.5
Ch/HA5%(1:7)	60:40	5
Ch/HA10%(1:7)	60:40	10

The ATR-FTIR spectra of Ch/HAGPhy1:7 membranes showed the characteristic bands of both polysaccharides and GPhy1:7 crosslinker (Fig. 45).

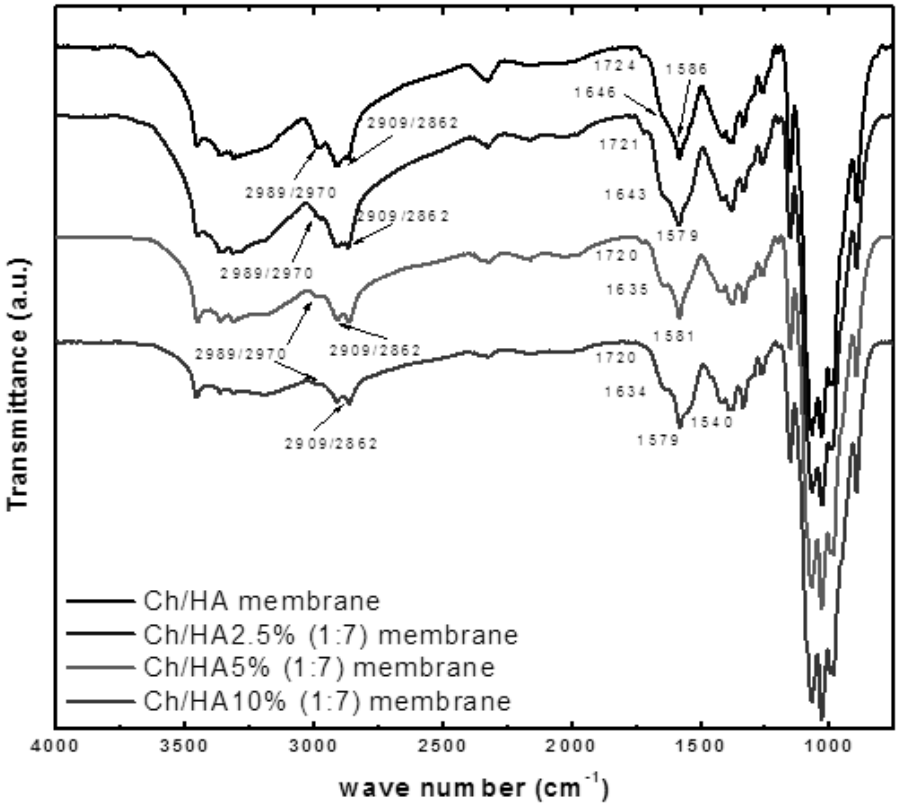

Figure 45 - ATR-FTIR spectra of Ch/HAGPhy1:7 membranes.

The main bands appeared: between 3600 and 3200 cm^{-1} (υ O-H and N-H associated); at 2924 and 2854 cm^{-1} (υ C-H); at 1720 cm^{-1} (υ C=O in carboxylic groups); at 1643/1634 cm^{-1} (υ C=O of amide, amide I); at 1579 cm^{-1} (δ N-H); at 1420 cm^{-1} (υ COO^- and δ C-H); at 1373 cm^{-1} (δ -CH_3 symmetrical); at 1333 cm^{-1} (υ C-N, amide III); at 1258/1262 cm^{-1} (υ P=O); at 1150 cm^{-1} (υ C-O-C asymmetric); at 1066, 1029, 995 and 984 cm^{-1} (υ C-O alcohols, υ P-O and P-O-C, υ C-O glycosidic linkages and vibration of pyranose structure); at 893 and 721 cm^{-1} (υ P-O and P-O-C). The main differences among spectra of Ch/HAGPhy1:7 membranes and that of Ch/HA membrane are as follows: disappearance of a shoulder with peaks at 2909-2862 cm^{-1}, which are more pronounced in the uncrosslinked Ch/HA membrane; in the range 1700-1500 cm^{-1}, an increase and shift in the band of amide I towards lower wavenumber (1643 to 1634 cm^{-1}) respect to uncrosslinked membrane (1646 cm^{-1}); the band at 1579 cm^{-1} shifted respect Ch/HA membrane (1586 cm^{-1}) as a consequence of ionic interactions between the NH_3^+ groups

of Ch/HAGPhy1.7 membrane and phosphate groups of GPh1:7; a change in the intensities of the bands in the range 1150 and 950 cm^{-1}.

Surface morphology and elemental composition of Ch/HAGPhy1:7 membranes were examined by SEM and EDX, respectively. Fig. 46 shows the SEM images of Ch/HAGPhy1:7 membranes. A highly porous well-structured morphology was observed in all samples. Porosity tends to decrease with the crosslinker content providing a network of reduced mesh size. This surface morphology seems to be very adequate for the colonization and proliferation of cells in tissue engineering applications.

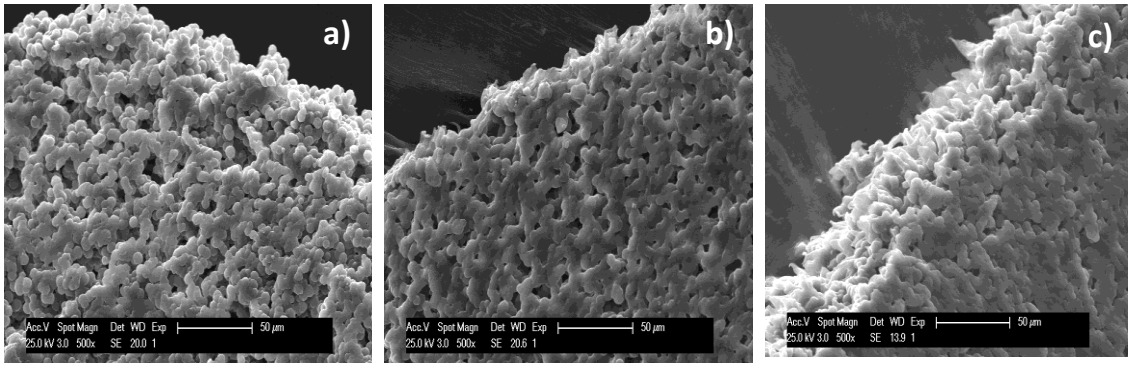

Figure 46 - SEM images of Ch/HAGPhy1:7 membranes of different crosslinker concentrations: a)Ch/HA2.5%(1:7), b)Ch/HA5%(1:7), c)Ch/HA10%(1:7)

The EDX spectra of Ch/HAGPhy1:7 membranes showed the peaks of the main elements C, O, N and P. EDX results are shown in Table 19. It can be clearly observed a decrease in the C/P ratio with the GPhy1:7 content in the membrane as well as a drop in the N/P ratio, confirming the crosslinking reaction.

Table 19 - EDX results of Ch/HAGPhy1:7 membranes.

Membrane	C/N	C/O	C/P	N/P
Ch/HA2.5%(1:7)	-	-	-	-
Ch/HA5%(1:7)	4.8	1.1	188	39
Ch/HA10%(1:7)	4.6	1.1	90	20

Thermal degradation of Ch/HAGPhy1:7 membranes were analysed by thermogravimetry. TGA and DTGA curves are shown in Table 20. The degradation patterns of all Ch/HAGPhy1:7 membranes were rather similar but they showed differences respect to the uncrosslinked Ch/HA membrane. Independent of GPhy1:7 concentration, degradation of

Ch/HAGPhy1:7 membranes took place in two main degradation steps whereas that of Ch/HA membranes in three steps. This difference makes it clear that both polysaccharides are basically mixed in the uncrosslinked membranes while they are well entangled forming semi-IPN networks in the Ch/HAGPhy1:7 membranes. Moreover, the T_{max} values in the semi-IPN samples are higher compared to Ch/HA sample, manifesting the crosslinked reaction and the formation of entanglements between both polysaccharides which in addition, can be stabilized with hydrophilic interactions. Considering the GPhy1:7 concentrations, the 5% one provided membranes having the highest stability while the 10% one gave rise to membranes with the lowest thermal stability.

Table 20 - Thermal degradation results of Ch/HAGPhy1:7 membranes under air atmosphere.

Sample	T_{max} (ºC)		
	1st step	2nd step	3rd step
Ch/HA	271	497	560
Ch/HA2.5%(1:7)	292	586	
Ch/HA5%(1:7)	286	602	
Ch/HA10%(1:7)	293	512	

Swelling behaviour of crosslinked membranes was studied in PBS of pH 7.4 at 37ºC. Evolution of swelling with time is displayed in Fig. 47. The Ch/HAGph1:7 membranes showed swelling profiles rather similar to those observed for ChGPhy1:7 membranes. Water uptake was very rapid, reaching the maximum between 1 and 2 days for all samples and giving values oscillating between 90 and 115%. The higher swelling was observed for the membrane crosslinked with 5% GPhy1:7, and the lower for that with 10% crosslinker, indicating again that 5% GPhy1:7 could be an optimum concentration. Afterwards, water uptake significantly decreased to values around 80-90% for the Ch/HA5%(1:7) and Ch/HA10%(1:7) membranes respectively, and around 70% for the Ch/HA2.5%(1:7) one. The swelling decrease can be attributed to some release of uncrosslinked HA chains but also to some breaking of ionic bonds, more pronounced for the samples fabricated with the lower crosslinker content.

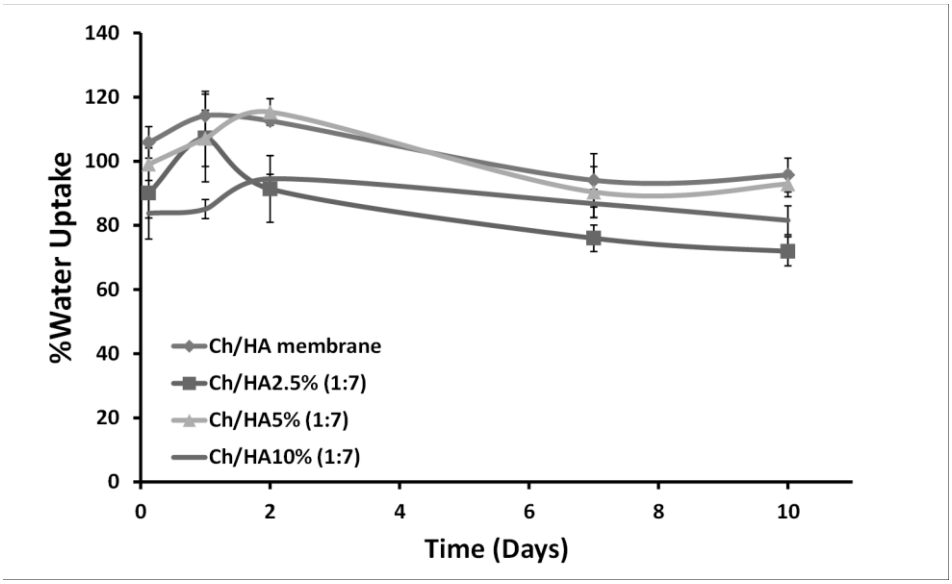

*Figure 47- Water uptake of Ch/HAGPhy1:7 membranes in PBS (pH 7.4, 37ºC). Results are given as mean ± sd (n=5). Statistical analysis (ANOVA) of each sample was performed at times 7 and 10 days with respect to 1 day (*p<0.05) and with respect to 2 days (#p<0.05).*

From swelling experiments results, we can say that both 5 and 10% GPhy1:7 concentrations provide membranes with adequate swelling behaviour and good stability for biomedical applications.

4.9 Formation of apatite-like layer on Ch membranes crosslinked with GPhy

Ch membranes crosslinked with 10% GPhy1:7 crosslinked named as Ch10%(1:7) membranes, were used for mineralization assays. The formation of an apatite-like layer on the surface of the membranes was studied with time by soaking the sample in SBF1.5 at 37ºC. Growth of an apatite-like layer was confirmed by experimental techniques such as SEM, EDX and ATR-FTIR. Fig. 48 shows the SEM photographs of the surface of Ch10%(1:7) membranes after 4, 7 and 14 days of soaking in SBF.1.5. At 4 days, the surface of the membranes showed precipitation of aggregates which were concentrated on localized zones, indicative of Ca-P deposits. At 7 days, the precipitates appeared more disseminated over the surface and at 14 days, the aggregates practically colonized the whole surface. At higher magnification (2000x), it could be appreciated that precipitates were formed by spherical particles that presented the typical coli flower morphology attributed to apatite-like layer. EDX spectra of the precipitates obtained at different periods of time showed the typical bands of Ca and P giving a Ca/P ratio of 1.39 within 4 days, value that approaches to that of Ca/P ratio of biological apatite (1.66).

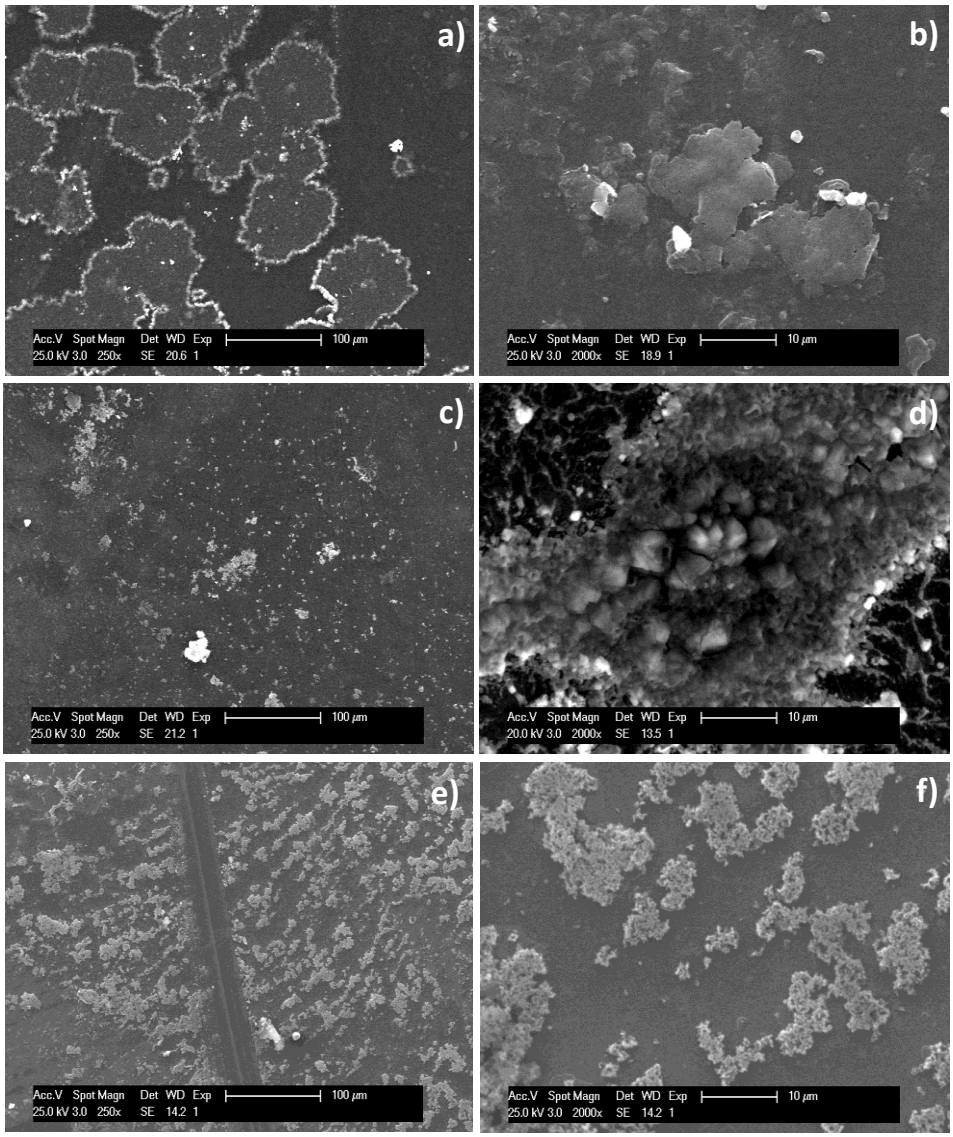

Figure 48 - SEM photographs of the Ch10%(1:7) membrane at 4 days (upper), 7 days (middle) and 14 days (bottom) of immersion in SBF1.5.

This finding suggests that the Ch membranes prepared with GPhy crosslinkers can have application in tissues regeneration processes involving bone, such as subchondral cartilage repair.

4.10 Biological behaviour of polysaccharide crosslinked membranes

In this example, biological behaviour of Ch and Ch/HA membranes fabricated with different GPhy crosslinkers were evaluated by respective MTT assays. Names and composition of membranes studied are summarized in Table 21.

Table 21 - Names and composition of Ch and Ch/HA membranes prepared with GPhy crosslinkers

Membrane family Name	Sample Name	Ch/HA (wt/wt)	GPhy Content (wt % respect to Ch)	Crosslinker Type
ChGPhy1:7	Ch2.5%(1:7)	100:0	2.5	GPhy1:7
ChGPhy1:7	Ch5%(1:7)	100:0	5	GPhy1:7
ChGPhy1:7	Ch10%(1:7)	100:0	10	GPhy1:7
Ch/HAGPhy1:7	Ch/HA2.5%(1:7)	60:40	2.5	GPhy1:7
Ch/HAGPhy1:7	Ch/HA5%(1:7)	60:40	5	GPhy1:7
Ch/HAGPhy1:7	Ch/HA10%(1:7)	60:40	10	GPhy1:7

Respect to membranes fabricated with only Ch, cytotoxicity results of ChGPhy1:7 membranes on human fibroblasts are shown in Fig. 49. It can be seen that cell viability in presence of extracts taken between 14 h and 14 d, was around or higher than 100 % indicating absence of cytotoxicity (ISO/EN10993-5, 2009).

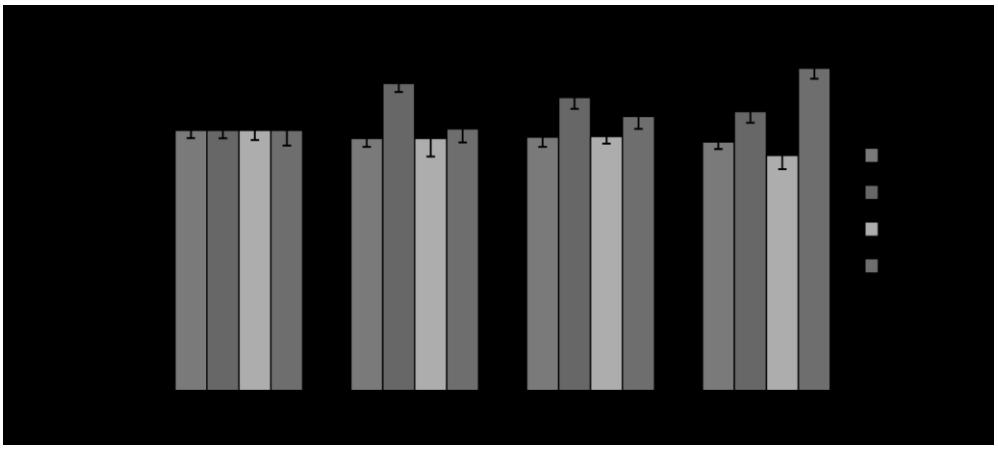

*Figure 49 - Cell viability results of human fibroblasts in presence of extracts of ChGPh1.7 membranes. Results are shown as mean ± sd (n=8). Significant differences (*p<0.05) of results of cements with respect to control are indicated in the graph.*

Cell proliferation on the ChGPhy1:7 membranes was quantitatively analysed after different times post-seeding and results are displayed in Fig. 50. For Ch10%(1:7) membranes cell proliferation notably increased with respect to Ch after 14 days post-seeding, indicating that the higher presence of the phytate derivative in this composition makes it more evident that this compound can have a stimulation activity on the proliferation of fibroblasts.

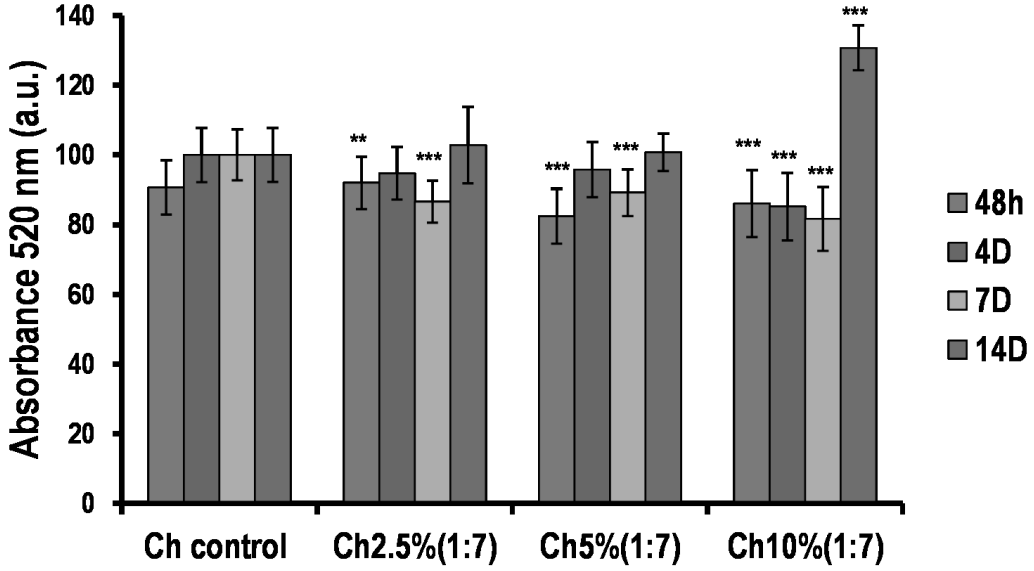

*Figure 50 - Alamar Blue results for ChGPh1.7 membranes. All the results are shown as mean ± sd (n=8). Asterisk depicts a significant difference between samples respect to control (**p< 0.005 and ***p<0.001).*

Morphology of cells adhered on ChGPh1.7 membranes was examined by SEM at different periods of time after seeding (Fig. 51). At 24 h the cells adopt spherical morphology on every membrane. However, after 4 days, more elongated cells were observed on ChGPhy1:7 membranes compared to those of plain Ch, and, after 7 and 14 days cell colonization was very good for ChGPhy1:7 membranes and qualitatively higher compared to those of Ch forming the typical monolayer, particularly more evident for the Ch10% (1:7) composition.

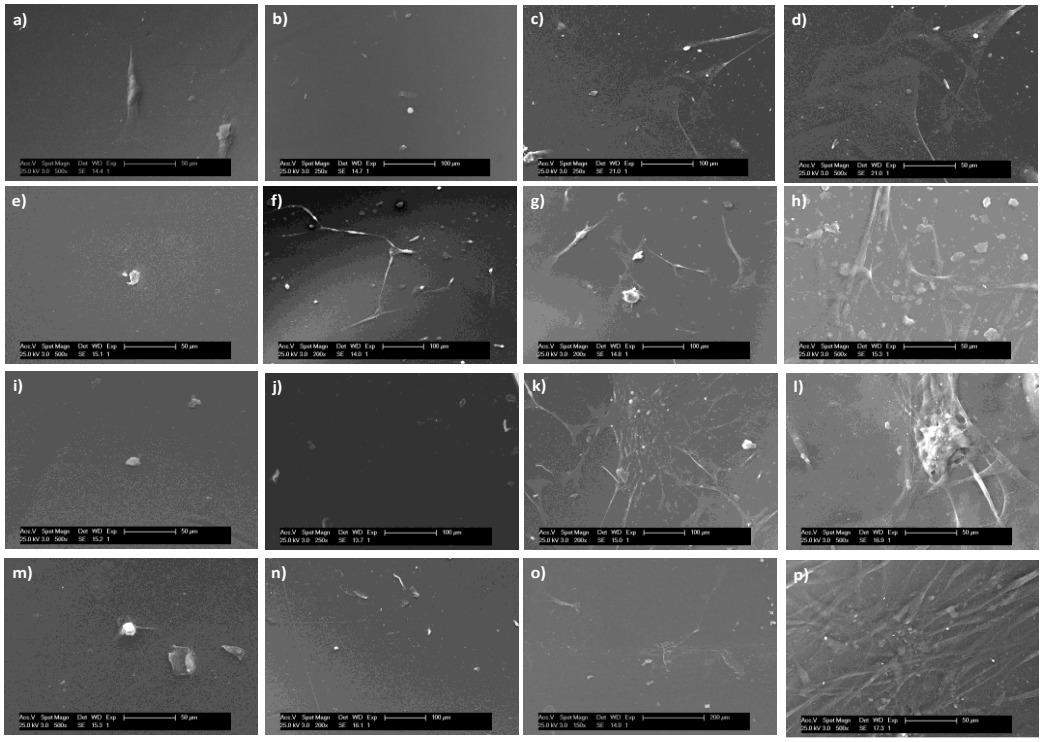

Figure 51 - SEM images of ChGPh1:7 membranes at 24 h (a-d), 4 (e-h), 7 (i-l) and 14 (m-p) days after human fibroblasts seeding for membranes of Ch (a-d), Ch2.5% (1:7) (e-h), Ch5% (1:7) (i-l) and Ch10% (1:7) (m-p) respectively.

Additionally, morphology of cell attached on ChGPhy1:7 membranes was analysed by optical microscopy and results are shown in Fig. 52. After 14 days of seeding, the epifluorescence microscopy images revealed elongated morphology of cells grown on all membranes but a denser meshwork was observed on the membranes of Ch10%(1:7) composition.

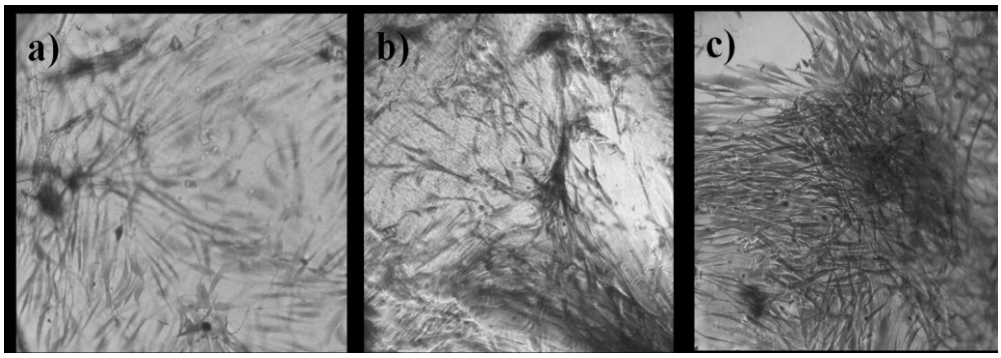

Figure 52 - Optical microscopy images of cell stained with Crystal attached on ChGPhy(1:7) membranes after 14 days human fibroblasts seeding. a) Ch2.5%(1:7), b) Ch5%(1:7), c) Ch10%(1:7).

As far as membranes fabricated with both Ch and HA, this membrane family was also biocompatible in the MTT test. Cell adherence and proliferation results are shown in Fig.53. Adherence and growth of fibroblasts on the Ch/HAGPhy1:7 membranes followed the same pattern as uncrosslinked Ch/HA membranes (control). Adherence was similar to control at 2 days. From then on until 14 days, cell proliferation significantly decreased to control for Ch/HA2.5(1:7) and Ch/HA5(1:7) membranes. However, for the Ch/HA5%(1:7) membrane fibroblasts growth was comparable to control, indicating that this composition would be the most indicated for application in regeneration processes.

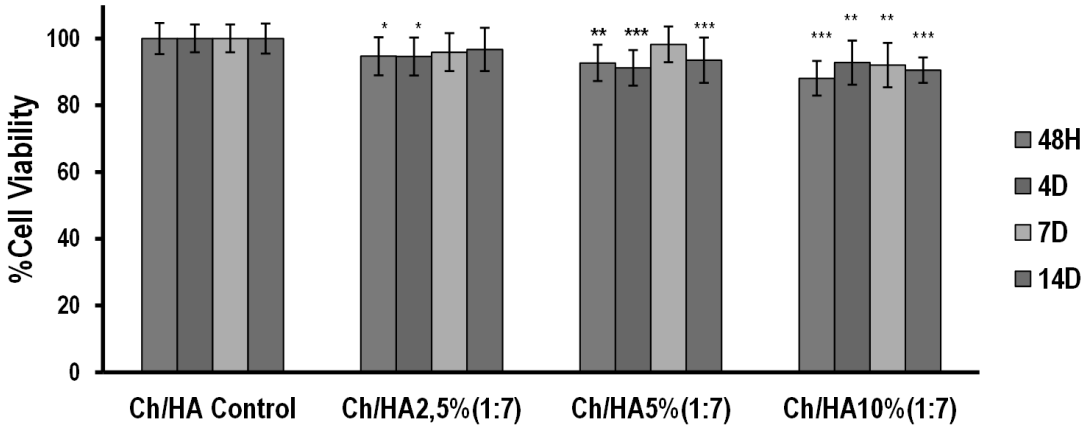

*Figure 53 - Cell viability results of human fibroblasts in presence of extracts of Ch/HAGPhy2.5% (1:7), Ch/HAGPhy5%(1:7) and Ch/HAGPhy10% (1:7) membranes. Results are shown as mean ± sd (n=8). Significant differences (*p<0.05) of results of cements with respect to control are indicated in the graph.*

Chapter 5 - Conclusions

The results from Part I show that for the first GPhy synthesis:

- Reaction between Glycerol and Phytic Acid was successful.
- GPhy has a higher thermal stability than β-GP.
- GPhy and β-GP were less cytotoxic than PA against fibroblasts and cytotoxicity of GPhy was comparable to that of β-GP. Fundamental for its utilisation as a crosslinking agent in the membranes prepared during this work.

The results from Part I show that for Ch/GPhy membranes:

- All membranes prepared were successfully crosslinked.
- The surface of chitosan membranes crosslinked with GPhy presented a smooth topography independent of their GPhy concentration.
- GPhy concentration doesn't seem to significantly affect membrane thermal stability.

The results from Part I show that for Ch:HA/GPhy membranes:

- All membranes prepared were successfully crosslinked;
- A highly porous well-structured morphology was observed in all samples independent on Ch:HA ratio and content of GPhy, this surface morphology seems to be very adequate for the colonization and proliferation of cells in tissue engineering applications;
- GPhy concentration doesn't seem to significantly affect membrane thermal stability.

The results from Part II show that for the second GPhy synthesis:

- The Gphy crosslinker synthetized is thermally stable;
- The biocompatibility of this GPhy crosslinker is higher when compared to other phytate crosslinkers currently used in literature, including β-GP.

The results from Part II show that for Ch/GPhy membranes:

- All membranes prepared were successfully crosslinked;
- The surface of chitosan membranes crosslinked with GPhy presented a smooth topography independent of GPhy concentration;
- GPhy concentration doesn't seem to significantly affect membrane thermal stability;
- Both 5 and 10% GPhy1:7 provided membranes with adequate swelling behaviour and stability to be used in biomedical applications;
- Formation of the apatite-like crystals was confirmed indicating that the Ch:HA membranes prepared with GPhy crosslinkers may have application in tissues regeneration processes involving bone, such as subchondral cartilage repair;
- Cytotoxicity assays on human fibroblasts show absence of cytotoxicity.

The results from Part II show that for Ch:HA/GPhy membranes:

- All membranes prepared were successfully crosslinked;
- The surface of these membranes showed a highly porous well-structured morphology. Porosity tends to decrease with the crosslinker content providing a network of reduced mesh size;
- Considering the GPhy1:7 concentrations, the 5% Ch:HA/GPhy one provided membranes having the highest thermal stability while the 10% one gave rise to membranes with the lowest stability;
- From swelling experiments results, we can say that both 5 and 10% GPhy1:7 concentrations provide membranes with adequate swelling behaviour and good stability for biomedical applications;
- Cytotoxicity assays on human fibroblasts show absence of cytotoxicity.

Chapter 6 - Future work

This work has been based on the synthesis of membranes based on hydrogels from natural polymers and the influence of these polymers on the final behavior of the membranes.

To follow up this study it is proposed to do the following steps:

- Long-term stability and degradation assays.
- Comprehensive characterization of rheological properties.
- Perform specific in vitro cell assays for the designed application.
- Study the behavior of these systems in vivo in animal models.

References

Anitha, A. et al., 2014. Chitin and chitosan in selected biomedical applications. *Progress in Polymer Science*, pp.1–24. Available at: http://dx.doi.org/10.1016/j.progpolymsci.2014.02.008.

Athanasiou, K.A., Eric, M.D. & C.Hu, J., 2009. *Articular Cartilage Tissue Engineering*, Morgan & Claypool.

Camp, C.L., Stuart, M.J. & Krych, A.J., 2014. Current concepts of articular cartilage restoration techniques in the knee. *Sports health*, 6(3), pp.265–73. Available at: http://www.ncbi.nlm.nih.gov/pubmed/24790697%5Cnhttp://www.pubmedcentral.nih.gov/articlerender.fcgi?artid=PMC4000472.

Crimella, T. et al., 1992. Determination of Purity of Commercially Available Inositol Hexaphosphate (Phytates) and Preparation of a Reference Material. In M. Magnani & J. R. DeLoach, eds. *The Use of Resealed Erythrocytes as Carriers and Bioreactors*. Boston, MA: Springer US, pp. 51–54. Available at: http://dx.doi.org/10.1007/978-1-4615-3030-5_6.

Croisier, F. & Jérôme, C., 2013. Chitosan-based biomaterials for tissue engineering. *European Polymer Journal*, 49(4), pp.780–792. Available at: http://dx.doi.org/10.1016/j.eurpolymj.2012.12.009.

Cui, X. et al., 2010. Electroless Ni – P plating with a phytic acid pretreatment on AZ91D magnesium alloy. *Materials Chemistry and Physics*, 121(1–2), pp.308–313. Available at: http://dx.doi.org/10.1016/j.matchemphys.2010.01.042.

Dash, M. et al., 2011. Chitosan - A versatile semi-synthetic polymer in biomedical applications. *Progress in Polymer Science (Oxford)*, 36(8), pp.981–1014. Available at: http://dx.doi.org/10.1016/j.progpolymsci.2011.02.001.

Falcone, S.J., Palmeri, D. & Berg, R.A., 2006. Biomedical Applications of Hyaluronic Acid. *Polysaccharides for Drug Delivery and Pharmaceutical Applications*, 20(1426–9686 (Print)), pp.155–174. Available at: http://pubs.acs.org/doi/abs/10.1021/bk-2006-0934.ch008.

Fernández-quiroz, D. et al., 2015. Effect of the molecular architecture on the thermosensitive properties of chitosan- g -poly (N -vinylcaprolactam). *Carbohydrate Polymers*, 134, pp.92–101. Available at: http://dx.doi.org/10.1016/j.carbpol.2015.07.069.

Govindaraju, V., Young, K. & Maudsley, A.A., 2000. Proton NMR chemical shifts and

coupling constants for brain metabolites. *NMR in Biomedicine*, 13(3), pp.129–153.

Graf, E. & Eaton, J.W., 1990. Antioxidant functions of phytic acid. *Free Radical Biology and Medicine*, 8(1), pp.61–69.

Haxaire, K. et al., 2003. Hydration of polysaccharide hyaluronan observed by IR spectrometry. I. Preliminary experiments and band assignments. *Biopolymers - Biospectroscopy Section*, 72(1), pp.10–20.

Ishiguro, T. et al., 2003. Rapid measurement of phytate in raw soymilk by mid-infrared spectroscopy. *Bioscience, biotechnology, and biochemistry*, 67(4), pp.752–7. Available at: http://www.ncbi.nlm.nih.gov/pubmed/12784614.

ISO/EN10993-5, 2009. B. *International Standard ISO 10993-5 Biological evaluation of medical devices - Part 5: Tests for cytotoxicity: in vitro methods*, 3 Ed, p.42.

Khor, E. & Lim, L.Y., Implantable applications of chitin and chitosan by Ellen Hackett on Prezi. Available at: http://prezi.com/c9i7%7B_%7D7fk%7B_%7Dozo/implantable-applications-of-chitin-and-chitosan/.

Kim, I.-Y. et al., 2008. Chitosan and its derivatives for tissue engineering applications. *Biotechnol. Adv.*, 26(1), pp.1–21. Available at: http://www.sciencedirect.com/science/article/pii/S0734975007000948.

Kuettner, K.E., 1992. Biochemistry of articular cartilage in health and disease. *Clinical Biochemistry*, 25(3), pp.155–163.

Kumar, M., 2000. A review of chitin and chitosan applications. *Reactive & Functional Polymers*, 46(1), pp.1–27.

L. Radin, E., 2004. Who Gets Osteoarthritis and Why? *The Journal of Rheumatology*.

Leach, J.B. et al., 2004. Development of photocrosslinkable hyaluronic acid-polyethylene glycol-peptide composite hydrogels for soft tissue engineering. *Journal of Biomedical Materials Research Part A*, 70A(1), pp.74–82.

Lee, H. et al., 2011. Oral delivery of insulin using chitosan capsules cross-linked with phytic acid. *Bio-Medical Materials and Engineering*, 21(1), pp.25–36.

Li, G. et al., 2013. Subchondral bone in osteoarthritis: insight into risk factors and microstructural changes. *Arthritis research & therapy*, 15(6), p.223. Available at: http://www.ncbi.nlm.nih.gov/pubmed/24321104.

Liao, Y.-H. et al., 2005. Hyaluronan: pharmaceutical characterization and drug delivery. *Drug delivery*, 12(6), pp.327–342.

Liu, L. et al., 2011. Microbial production of hyaluronic acid: current state, challenges, and

perspectives. *Microbial cell factories*, 10(1), p.99. Available at: http://www.pubmedcentral.nih.gov/articlerender.fcgi?artid=3239841&tool=pmcentrez&rendertype=abstract.

Madry, H., van Dijk, C.N. & Mueller-Gerbl, M., 2010. The basic science of the subchondral bone. *Knee Surgery, Sports Traumatology, Arthroscopy*, 18(4), pp.419–433.

Martin, J.B. et al., 1987. Identification of inositol hexaphosphate in 31P-NMR spectra of Dictyostelium discoideum amoebae. Relevance to intracellular pH determination. *BBA - Molecular Cell Research*, 931(1), pp.16–25.

Montgomery, S.R. et al., 2014. Trends in the surgical treatment of articular cartilage defects of the knee in the United States. *Knee surgery, sports traumatology, arthroscopy : official journal of the ESSKA*, 22(9), pp.2070–2075.

Necas, J. et al., 2008. Hyaluronic acid (hyaluronan): A review. *Veterinarni Medicina*, 53(8), pp.397–411.

Nooeaid, P. et al., 2012. Osteochondral tissue engineering: Scaffolds, stem cells and applications. *Journal of Cellular and Molecular Medicine*, 16(10), pp.2247–2270.

Nukavarapu, S.P. & Dorcemus, D.L., 2013. Osteochondral tissue engineering: Current strategies and challenges. *Biotechnology Advances*, 31(5), pp.706–721. Available at: http://dx.doi.org/10.1016/j.biotechadv.2012.11.004.

O'Neill, I.K., Sargent, M. & Trimble, M.L., 1980. Determination of phytate in foods by phosphorus-31 Fourier transform nuclear magnetic resonance spectrometry. *Anal Chem*, 52(8), pp.1288–1291. Available at: http://www.ncbi.nlm.nih.gov/pubmed/7447023.

Oatway, L., Vasanthan, T. & Helm, J.H., 2001. Phytic acid. *Food Reviews International*, 17(May 2013), pp.419–431.

Oliveira, I.R. De et al., 2015. Characterization of Calcium Aluminate Cement Phases when in Contact with Simulated Body Fluid 2 . Experimental Procedures. , 18(2), pp.382–389.

Panseri, S. et al., 2012. Osteochondral tissue engineering approaches for articular cartilage and subchondral bone regeneration. *Knee Surgery, Sports Traumatology, Arthroscopy*, 20(6), pp.1182–1191.

Ravichandran, R. et al., 2013. Mimicking Native Extracellular Matrix with Phytic Acid-Crosslinked Protein Nanofibers for Cardiac Tissue Engineering. *Macromolecular Bioscience*, 13(3), pp.366–375.

Shu, X.Z. & Zhu, K.J., 2002a. Controlled drug release properties of ionically cross-linked chitosan beads: the influence of anion structure. *European Journal of Pharmaceutics and*

Biopharmaceutics, 233(2), pp.217–225.

Shu, X.Z. & Zhu, K.J., 2002b. The influence of multivalent phosphate structure on the properties of ionically cross-linked chitosan films for controlled drug release. *European Journal of Pharmaceutics and Biopharmaceutics*, 54(2), pp.235–243.

Sophia Fox, A.J., Bedi, A. & Rodeo, S.A., 2009. The basic science of articular cartilage: structure, composition, and function. *Sports health*, 1(6), pp.461–8. Available at: http://www.pubmedcentral.nih.gov/articlerender.fcgi?artid=3445147&tool=pmcentrez&rendertype=abstract.

Turner, B.L., Mahieu, N. & Condron, L.M., 2003. Phosphorus-31 Nuclear Magnetic Resonance Spectral Assignments of Phosphorus Compounds in Soil NaOH–EDTA Extracts. *Soil Science Society of America Journal*, 67(2), pp.497–510.

Versier, G. & Dubrana, F., 2011. Treatment of knee cartilage defect in 2010. *Orthopaedics and Traumatology: Surgery and Research*, 97(8 SUPPL.), pp.140–153.

Zargar, V., Asghari, M. & Dashti, A., 2015. A Review on Chitin and Chitosan Polymers : Structure , Chemistry , Solubility , Derivatives , and Applications. , (3), pp.204–226.

Zhang, L., Hu, J. & Athanasiou, K.A., 2009. The role of tissue engineering in articular cartilage repair and regeneration. *Critical reviews in biomedical engineering*, 37(1–2), pp.1–57. Available at: http://www.pubmedcentral.nih.gov/articlerender.fcgi?artid=3146065&tool=pmcentrez&rendertype=abstract.